The People's Democratic Republic of Algeria

University of Saad Dahlab Blida 1

Institute of Aeronautics and Space Studies

Air Navigation Department

Master's Degree

Specialty : CNS/ATM

Attitude Determination And Control System Of CubeSat

BY

Zebdi Ishak Islam

Kermali Mohammed

proposed and directed by : Rahmouni Mohammed

Blida, June 2024

Abstract

This thesis presents the simulation and analysis of attitude determination and control for a CubeSat using reaction wheels. CubeSats, small standardized satellites, are increasingly popular for space missions due to their cost-effectiveness and versatility. Precise attitude control is essential for mission success, enabling accurate orientation for tasks such as imaging, communication, and scientific experiments.

Our study focuses on developing a comprehensive simulation model that integrates attitude determination algorithms and reaction wheel-based control mechanisms. The simulation environment, created using MATLAB, includes detailed modeling of the CubeSat's dynamics, environmental disturbances, and sensor noise. Key elements of the control system , the proportional-integral-derivative (PID) controller, are implemented to achieve desired orientation stability and accuracy.

Résumé

Cette thèse présente la simulation et l'analyse de la détermination et du contrôle d'attitude d'un CubeSat utilisant des roues de réaction. Les CubeSats, petits satellites standardisés, sont de plus en plus populaires pour les missions spatiales en raison de leur rentabilité et de leur polyvalence. Un contrôle précis de l'attitude est essentiel au succès de la mission, permettant une orientation précise pour des tâches telles que l'imagerie, la communication et les expériences scientifiques.

Notre étude se concentre sur le développement d'un modèle de simulation complet intégrant des algorithmes de détermination d'attitude et des mécanismes de contrôle basés sur des roues de réaction. L'environnement de simulation, créé à l'aide de MATLAB, comprend une modélisation détaillée de la dynamique du CubeSat, des perturbations environnementales et du bruit des capteurs. Les éléments clés du système de

contrôle, le contrôleur proportionnel-intégral-dérivé (PID), sont mis en œuvre pour obtenir la stabilité et la précision d'orientation souhaitées.

ملخص

تقدم هذه الأطروحة محاكاة وتحليل تحديد الاتجاه والتحكم للقمر CubeSat باستخدام عجلات التفاعل. تحظى CubeSats ، وهي أقمار صناعية صغيرة موحدة المعايير، برواج في المهام الفضائية نظرًا لفعاليتها من حيث التكلفة وتعدد استخداماتها. يعد التحكم الدقيق في الموقف أمرًا ضروريًا لنجاح المهمة، مما يتيح التوجيه الدقيق لمهام مثل التصوير والاتصالات والتجارب العلمية.

تركز دراستنا على تطوير نموذج محاكاة شامل يدمج خوارزميات تحديد الاتجاه وآليات التحكم القائمة على عجلة التفاعل. تتضمن بيئة المحاكاة، التي تم إنشاؤها باستخدام MATLAB ، نماذج تفصيلية لديناميكيات CubeSat ، والاضطرابات البيئية المحيطة، وضوضاء أجهزة الاستشعار. يتم تشغيل العناصر الرئيسية لنظام التحكم، وحدة التحكم المتناسبة والتكاملية والمشتقة (PID) ، لتحقيق الاستقرار والدقة المطلوبة في التوجيه.

Acknowledgement

First and foremost, we would like to express our sincere gratitude to our advisor, Rahmouni Mohammed, for their continuous support, patience, and guidance throughout our research. Their insightful feedback and encouragement have been invaluable in the completion of this thesis. A special thanks to our colleagues and friends, for their support and companionship throughout this journey. Your encouragement and discussions have been a source of motivation and inspiration. we extend my heartfelt thanks to our family, especially our parents, and our siblings, for their unwavering support and belief in us. Their love and encouragement have been our greatest strength.

To anyone who has contributed to our academic journey and this thesis, whether mentioned here or not, please know that your support and contributions have been deeply appreciated.

Contents

List of Figures

List of Tables

List of Abbreviations and Symbols

Abbreviations

LEO	Low Earth Orbit
ADACS	Attitude Determination and Control System
IR	Infrared
P-POD	Poly-Picosatellite Orbital Deployer
NASA	National Aeronautics and Space Administration
ECEF	Earth-Centered, Earth-Fixed
RPY	Roll, Pitch, and Yaw
NED	North, East, Down
CSS	Coarse Sun Sensors
EHS	Earth Horizon Sensors
FSS	Fine Sun Sensors
MOI	Moment of Inertia
COG	Center of Gravity
GNC	Guidance, Navigation, and Control
GPS	Global Positioning System
LLH	latitude,longitude, altitude)
EMM2015	Earth Magnetic Model
EGM2008	Earth Gravitational Model
ECI	Earth-Centered Inertial
ENV	East, North, Vertical
INS	Inertial Navigation System
IMU	Inertial Measurement Unit
DOF	Degrees of Freedom

IGRF	International Geomagnetic Reference Field
PD	Proportional Derivative
PID	Proportional–integral–derivative
ISS	International Space Station
DOD	Department of Defense.
GEVS	General Environmental Verification Standard
GEO	Geosynchronous equatorial orbit

Symbols

x, y, z	Components of the mass center position vector in the inertial frame (m)
ϕ, θ, ψ	Euler roll, pitch, and yaw angles (rad)
q_0, q_1, q_2, q_3	Quaternions
u, v, w	Components of the mass center velocity vector in the body frame (m/s)
p, q, r	Components of the mass center angular velocity vector in the body frame (rad/s)
ω_{BI}	Angular velocity vector of the vehicle in the body frame (rad/s)
T_{IB}	Rotation matrix from frame I to frame B
H	Relationship between angular velocity components in body frame and derivative of Euler angles
m	Mass (kg)
I	Mass moment inertia matrix about the mass center in the body frame ($\mathrm{kg} \cdot \mathrm{m}^2$)
X, Y, Z	Components of the total force applied to CubeSAT in body frame (N)
L, M, N	Components of the total moment applied to CubeSAT in body frame ($\mathrm{N} \cdot \mathrm{m}$)
$r_{A \to B}$	Position vector from a generic point A to a generic point B (m)
V_{AB}	Velocity vector of a generic point A with respect to a generic frame B (m/s)
$\mathbf{S}(r)$	Skew symmetric matrix operator on a vector.Multiplying this matrix by a vector is equivalent to a cross product
X_i, Y_i, Z_i	Components of the total force applied to aircraft i in body frame (N)
L_i, M_i, N_i	Components of the total moment applied to aircraft i in body frame ($\mathrm{N} \cdot \mathrm{m}$)
g	Gravitational constant on Earth ($\mathrm{m/s}^2$)
ρ	Atmospheric density ($\mathrm{kg/m}^3$)

$S_B(r)$	Skew symmetric matrix operator on a vector expressed in the body frame
K_p, K_d, K_I	Proportional, derivative, and integral control gains
V	Total airspeed (m/s)
$\hat{p}, \hat{q}, \hat{r}$	Non-dimensional angular velocities
l	Distance from center of mass to aerodynamic center of the tail (m)
l_t	Distance from aerodynamic center of main wing to aerodynamic center of tail (m)

Introduction

This report represents aerospace mechanics and controls for CubeSats. A CubeSAT is a small satellite on the order of 10 centimeters along each axis. A 1U satellite is a small cube with 10 cm sides. These satellites are used for a variety of missions and created by a variety of different organizations. When deployed from a rocket, a CubeSAT may obtain a large angular velocity which must be reduced before most science missions or communications can take place. Maximizing solar energy charging also involves better pointing accuracy. To control the attitude of these small satellites, reaction wheels, magnetorquers and even the gravity gradient are used in low earth orbit (LEO) while reaction control thrusters are typically used in deep space. On a standard LEO CubeSAT, 3 reaction wheels are used as well as 3 magnetorquers. In the initial phase of the CubeSAT mission, the magnetorquers are used to reduce the angular velocity of the satellite down to a manageable level. Once the norm of the angular velocity is low enough, the reaction wheels can spin up reducing the angular velocity to zero. At this point a Sun finding algorithm is employed to find the Sun and fully charge the batteries. In LEO two independent vectors are obtained, the Sun vector and the magnetic field vector, to determine the current attitude of the vehicle which is typically called attitude determination. Other sensors such as horizon sensors, star trackers and even lunar sensors can be used to obtain the quaternion of the vehicle. This paper investigates the necessary mathematics to understand the intricacies of guidance, navigation and control specifically discussing the attitude determination and controls subsystem (ADACS).

Chapter 1

History and Comprehensive Overview of CubeSats and ADACS

Background

Orbital spacecraft have attracted significant global attention since before the launch of the first purpose-built satellite, Sputnik I, in 1957. The desire to deploy orbital craft for both manned and unmanned missions has been steadily growing since then. Initially focused on achieving reliable orbital flight, the industry has now shifted towards utilizing space for logistics, navigation, and communications, necessitating continuous advancements in spacecraft technology. Alongside the miniaturization of electronic components, the past two decades have witnessed a rise in the number of smaller spacecraft launches, particularly those following the CubeSat standard. While the CubeSat standard has gained popularity, the increase in commercial suppliers of CubeSat components has driven costs down for programs, albeit requiring additional effort to assess the performance and suitability of these new components. Among these new components, the demand for dependable and precise Attitude Determination and Control Systems (ADACS) to manage spacecraft orientation has emerged as a key focus for evaluation.

1.1 History of CubeSats

With the rise of space travel, exploration, and technology accessibility to the general public, the opportunities for advancements in Space and from Space are expanding. The utilization of Space-based Worldwide internet can provide connectivity to populations worldwide, especially in areas where terrestrial systems are too costly. Space-based communications can facilitate seamless scheduling from ships to harbors, eliminating the need for repeaters and streamlining logistics. Additionally, Space-based infra-red (IR) cameras can detect wildfire hotspots in challenging terrains, improving the efficiency and safety of wildland firefighters. As the demand for robust Space platforms grows, new and innovative missions are on the horizon. To meet the increasing complexity of mission requirements, advancements in subsystem components and new space platform architectures are essential. The emergence of CubeSat standards offers a promising solution for realizing complex missions through existing CubeSat architectures.The inception of the CubeSat standard can be traced back to 1999 when professors Jordi Puig-Suari from California Polytechnic State University and Bob Twiggs from Stanford University proposed itto satisfy the requirements for usage in the Poly-Picosatellite Orbital Deployer (P-POD)[**1**]. Their aim was to provide university students with the opportunity to create, construct, test, and operate uncomplicated spacecraft. In 2003, the first CubeSat was launched, followed by the inaugural NASA CubeSat, GeneSat-1, in 2006. The triumph of GeneSat-1 played a crucial role in the growing popularity of CubeSats. Initially, until 2013, CubeSats were primarily associated with academic and university projects. However, after 2013, the majority of CubeSats launched were intended for amateur or commercial purposes. In 2012, only 72 CubeSats were in orbit, but by January 2019, over 900 had been successfully deployed , as of 2024 May 31 2396 cubesats have been launched in space [**2**]. The utilization of these satellites continues to expand with each passing year[**3**].

1.2 Defining CubeSats

cubesats are generally considered small satellites, but they are often categorized differently as shown in Table 1.1 by mass[**4**].

Nanosatellite	<10kg
Microsatellite	10-100kg
Minisatellite	100-500kg
Small Satellite	500-1000kg
Large Satellite	>1000kg

Table 1.1: First satellite classification

Mass is used as a simplified measurement for classification, providing a reference to the size of the spacecraft being developed. The main objective of standardization is the structure of the CubeSat. A single CubeSat unit, or "U," is a 10cm x 10cm x 10cm cube weighing approximately 1 to 1.5 kg. By combining multiple "U's," standardized configurations can be effectively built. The most popular configurations currently in use are the 1U, 3U, and 6U form factors and these are shown in figure 1.1. These configurations have gained popularity due to the availability of standardized CubeSat deployment systems. Examples of such systems include the P-POD and Planetary Systems Corporation's Canisterized Satellite Deployer. By transferring the responsibility of developing the dispensing method and mechanism to another entity with flight heritage, the spacecraft development team can focus on satellite development while adhering to the standardized dispenser configuration.

The standardization of CubeSat structure was initially established in 1999, and the CubeSat Design Specification is currently on revision 13[**5**]. As a result, multiple commercial entities have started developing standardized components specifically for CubeSats. By adhering to these standards, development efforts and rework inefficiencies can be reduced, leading to cost savings that can be passed on to satellite developers. Lower costs also lower the barrier for entry into space, allowing a greater number of organizations to develop space missions using CubeSats as the base platform.

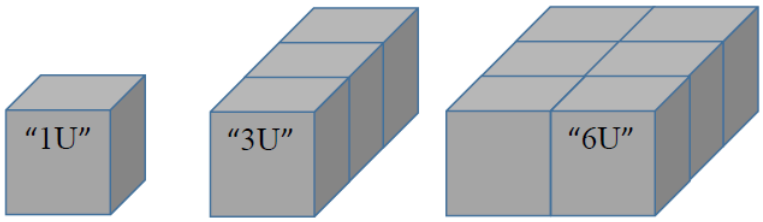

Figure 1.1: Standard 1U, 3U, and 6U CubeSat Configurations

1.3 Attitude Determination and Control System

Quantitative measurements are essential for attitude determination and control. To achieve accurate synchronization, it is crucial to establish a common frame of reference. When describing spacecraft attitude, six variables are used to represent the six degrees of freedom. Three variables define the spacecraft's position within the orbit relative to an external origin or fixed frame. For these measurements, the approximate center of the Earth is typically chosen as the reference point. The Z axis aligns with the true North Pole, the X axis intersects the Equator and the Prime Meridian, and the Y axis is orthogonal to both the Z and X axes. The positive direction of the Y axis follows the right-hand rule for the cross product of the Z and X components, as depicted in Figure 1.2.

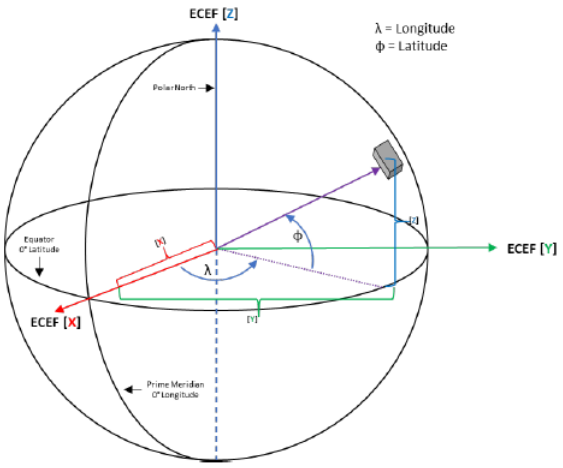

Figure 1.2: Earth Centered, Earth Fixed coordinate system

This reference frame, known as Earth-Centered, Earth Fixed (ECEF), originates

from the approximate Earth's core. The three variables in the ECEF frame are measured in terms of latitude, longitude, and distance from the origin at the Earth's core. It is important to note that the rotation of the ECEF frame is referenced to the celestial field, not the sun. Therefore, when making future calculations, time should be measured in sidereal time rather than solar time [**6**].

The three remaining parameters define the spacecraft's designated body frame. This frame is established during the chassis production, typically connected to a physical component of the chassis, and serves as the reference point for the onboard subsystems to determine their positioning. For instance, the solar panels are known to be attached to the -Y face, and aligning this face with the Sun pointing vector ensures optimal charging. By applying a coordinate transformation from the body frame, the orientation can be converted into the ECEF coordinate system for ground station relevance. These parameters, known as Roll, Pitch, and Yaw (RPY), collectively describe the spacecraft's attitude through rotations around the three primary axes. Roll represents the rotation around the X axis, Pitch around the Y axis, and Yaw around the Z axis as shown in figure 1.3.

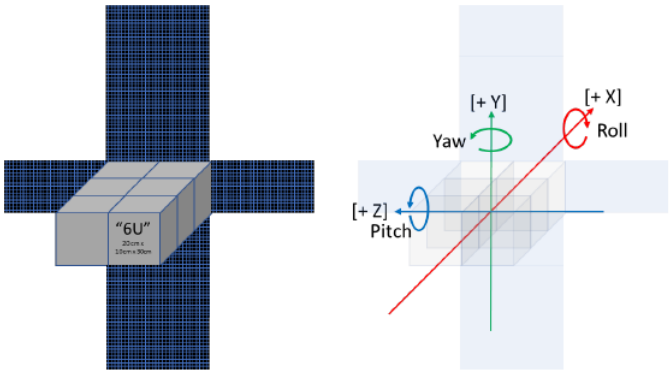

Figure 1.3: Primary axis Roll, Pitch, and Yaw

Additional transformations can be applied to the initial coordinate frames for specific purposes, such as ground station pointing. In this case, a North, East, Down (NED) system can be established as shown in figure 1.4, which is measured from any point on Earth.

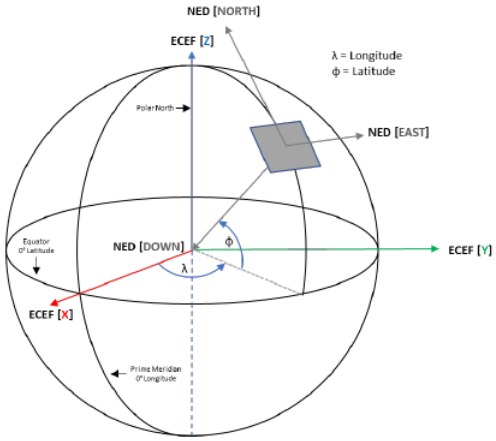

Figure 1.4: NED coordinate system overlaid on ECEF

This system utilizes Earth's magnetic field to align North with polar North, East with polar East, and Down with a direct pointing towards Earth's center. Once the reference frames are agreed upon, the latitude, longitude, and altitude with respect to the Earth-Centered, Earth-Fixed (ECEF) frame, along with the spacecraft's body frame yaw, pitch, and roll, can be transformed into the Earth-Centered, Earth-Fixed, Earth-Fixed (ECFEF) frame. This transformation allows for the discussion of Attitude Determination and Control System (ADACS) performance. ADACS has two primary functions: determining the spacecraft's attitude with respect to a specified frame and controlling the spacecraft's attitude or pointing. Both functions are crucial, but the determination of attitude from ADACS is a necessary input for the control function.

1.3.1 Attitude Determination

The trend towards expanded on-orbit operations , necessitates systems and subsystems like ADACS to advance into more intricate configurations of hardware and software to remain relevant. The emphasis on on-orbit maneuverability in CubeSats demands precise knowledge of spacecraft orientation in space, leading to continuous advancements in the determination aspect of ADACS. Attitude determination involves mathematically describing the spacecraft's orientation in relation to a specified reference frame, often linked with attitude estimation, which predicts the spacecraft's attitude at a specific time step. While determination and estimation offer similar data

to users, the derivation methods differ significantly in terms of error, computational complexity, and speed.

1.3.2 Attitude Determination Sensors

The precision of a spacecraft's attitude solution is influenced by both the effectiveness of the determination algorithm and the precision of the sensors that provide measurement data. As determination algorithms advanced in capability and complexity, the capacity to incorporate more data through additional sensor inputs also improved. The option to include more sensors led to advancements in sensor development. The proliferation and miniaturization of onboard computing enabled the creation of smaller and more intricate attitude sensors. When combined with the more robust algorithms, these advancements allow the ADACS to enhance the accuracy of the determination solution. This section provides a summary of the most frequently used ADACS determination sensors.

Sun Sensor

commonly have Sun Sensors, which are primarily Coarse Sun Sensors (CSS). CSS are essentially photoelectric cells that convert photon energy into electrical current. This current is then measured and converted into a digital signal. The digital signal corresponds to the location of the sensor on the spacecraft frame and indicates the intensity of the incoming light on that plane. By using multiple CSS on different planes along the positive and negative X, Y, and Z axes, it is possible to determine the 3-dimensional sun pointing vector, which can then be utilized by the ADACS system.

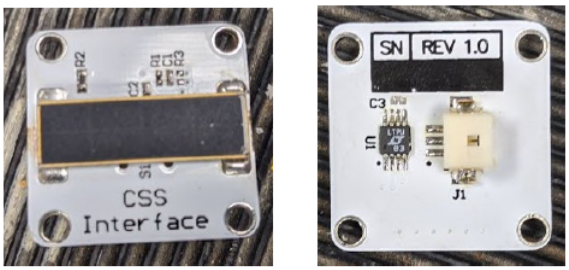

Figure 1.5: Solar-Cell type Coarse Sun Sensor, top and bottom view

Magnetometer

Spacecraft magnetometers are instruments used to detect magnetic fields. They consist of wound coils that detect changes in current caused by variations in the magnetic field. Magnetometers offer two types of data to an ADACS. The first type is a general measurement of the magnetic field in relation to the magnetometer's frame of reference. This, combined with the known values of Earth's magnetic field and any magnetic fields associated with the spacecraft, can determine a pointing vector. Additionally, by measuring changes in the field's value and rate of change, the ADACS can determine the spacecraft's degree and rate of rotation. While multiple axis magnetometers are available, simpler ADACS systems utilize single unidirectional magnetometers on each primary axis.

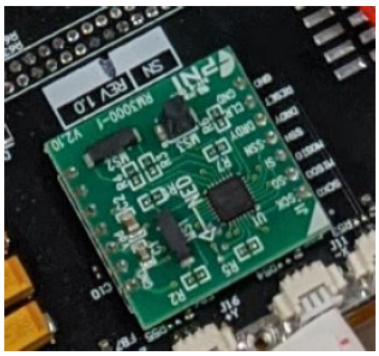

Figure 1.6: Magnetometer Board

Gyroscopes

Gyroscopes on spacecraft are widely used and efficient sensors for calculating the spacecraft's angular rate of change. These gyroscopes can be based on physical spinning plates or optical sensing systems, and can have either a single axis or multiple axes. Regardless of the type, the change in velocity of the spinning mass or the time taken for a photon to travel a known path is measured over time to determine the spacecraft's rate of change in rotation. By having a single axis gyroscope on each primary axis, the overall rotation rate of the spacecraft can be accurately calculated.

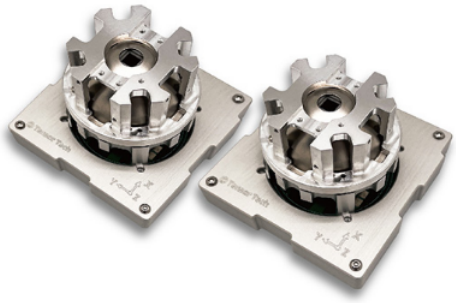

Figure 1.7: sensor Tech CMG-20m Control Moment Gyroscope

Star Trackers

Star trackers, also known as star cameras, are optical sensors that offer both the rate of change and a directional pointing vector to the ADACS. Recent technological advancements have allowed star trackers to utilize pre-loaded a-priori star fields for their current operations. These sensors collect imaging data from the celestial field onto an imaging plane and calculate the pointing vector using a comparative algorithm based on the known star field. As rotational sensors, star trackers can determine the rotation rate of their body frame around the observed star field pattern after the initial capture. They are typically the most accurate input sensors for the ADACS. While there are other sensors like Earth Horizon Sensors (EHS) and Fine Sun Sensors (FSS) available to spacecraft developers, star trackers are often preferred for their ease of use and capabilities. It is crucial to ensure the precise orientation of the sensor for an accurate determination solution, as any deviation from the prescribed axis can lead to errors in the attitude solution.

Figure 1.8: ST200 - CubeSat Star Tracker

1.3.3 Attitude control

The Control Function is the second primary function of the Attitude Determination and Control System (ADACS). Control refers to the ability to maneuver or re-orient the spacecraft to a specific location within a designated reference frame. In the case of a CubeSat-level ADACS, maneuvering may not be necessary, but orientation remains important. To fully orient a spacecraft, certain variables must be known to satisfy force or torque equations. The ADACS determination function requires knowledge of the spacecraft's current attitude and rates of rotation. The spacecraft's mass, Center of Gravity (COG), and Moment of Inertia (MOI) are typically stored values in the flight software, which can be updated as fuel is depleted. These values are necessary for calculating control forces around the spacecraft's body frame. Additionally, a frame of reference is required when commanding the target attitude and may need to be transformed for coordinate purposes. Controlling the spacecraft's attitude can become complex due to potential errors and coordinate transforms between components. Each sensor and control component has its own reference frame, and variations in mounting locations and orientations within the ADACS unit or chassis need to be mapped to a known frame of reference. Perturbations in space, such as 3rd body gravitational pull, atmospheric drag in Low Earth Orbits (LEO) as shown in figure 1.9 from [**7**] , magnetic deviations caused by Earth's precession, solar wind, and others, introduce additional errors. Even small deviations in pointing accuracy, when compounded over long distances in space missions, can result in significant deviations in physical distance. Therefore, the development of precise and accurate components for spacecraft control is crucial.

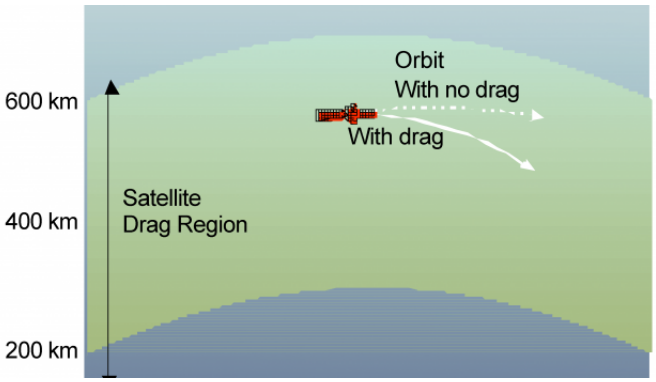

Figure 1.9: Satellite Drag

1.3.4 Attitude Control Components

The control function computes the force or torque value necessary to adjust the spacecraft's orientation. This value depends on the physical properties allowed by the control mechanisms, such as weight and maximum rotation rate of reaction wheels. The mechanism's location within the frame and its relation to the MOI are crucial for moment arms and torque applications. Additionally, the physical pointing of the mechanism, as in the case of thrusters, is also taken into account. These dependencies collectively impact the Force or Torque value needed to change the spacecraft's attitude, highlighting the importance of efficiencies. Although not covered in this study, the optimization of spacecraft control is a growing field that contributes to the continuous improvement of ADACS performance. Current optimization methods being explored include extensive research on machine learning[8] and the application of stochastic optimization algorithms to control issues . Reaction wheels and magnetorquers are common control components found in commercially available ADACS. While thrusters are typically used in larger spacecraft for attitude adjustments and station keeping, they are now being adopted in CubeSats, although the limited fuel capacity onboard makes them less ideal for attitude control.

Reaction Wheels

Reaction wheels operate when electrical motors rotate a weighted wheel within the spacecraft chassis creating a stored momentum value. When a brake is applied to the wheel the momentum is transferred into the body of the spacecraft thus imparting a torque to rotate the spacecraft. Common practice is to align a single reaction wheel on each of the three primary axes thereby allowing for control in all three planes of motion. Alternatively, if the spacecraft is rotating and needs to be slowed the wheel can be commanded to spin in the opposite direction, and when the braking action is applied the torque from the spacecraft body is negated by the opposing torque from the reaction wheel slowing the rate of rotation of the spacecraft. The variation of the rate of rotation of the reaction wheel up to a maximum value can be infinitely controllable, and as such the level of applied torques from the wheels to the spacecraft can be finely tuned. A weakness of reaction wheels is that they have an upper limit of rotation rate and can become saturated requiring additional control componentry to support

momentum shedding or dumping maneuvers.

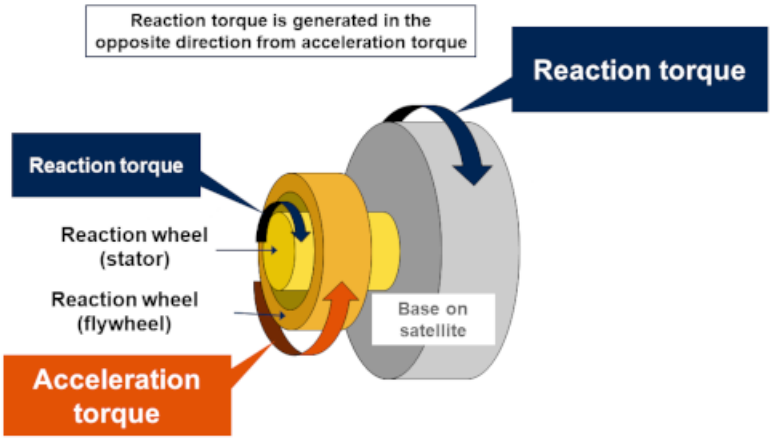

Figure 1.10: reaction wheel for cubesat

Magnetorquers

Also known as magnetic torque rods, function based on the concept of magnetic dipole moments. The control process begins by passing an electric current through a magnetic coil that is attached to the spacecraft, thereby generating a magnetic field within the spacecraft. When this magnetic field interacts with the Earth's ambient magnetic field, it creates a force that acts upon the center of gravity of the spacecraft, providing the necessary torque for rotation. Similar to reaction wheels, magnetorquers are installed along each primary axis, enabling control of the spacecraft's motion in three planes. The strength of the generated magnetic field can be adjusted by varying the current applied to the coils, allowing for the tuning of torque to the desired levels. By reversing the current flow through the coils, the dipole of the generated field can be reversed, resulting in torques in both positive and negative directions along the specified axis. Although magnetorquers consume very little power, they may require a significant amount of time to exert a substantial torque on the spacecraft.

Figure 1.11: ISIS-iMTQ-3-axis-magnetorquer

1.4 CubeSat Dynamics and its process of control

The control of a CubeSat's dynamic motion involves managing both translational and rotational aspects. Translational motion, which is akin to orbital motion, treats the satellite as a point mass and requires determining its orbital position through ground observation or on-board instruments. Orbital mechanics are used to propagate the satellite's orbital motion, with perturbation effects considered for accurate orbit prediction. Parameters like altitude and inclination are adjusted through orbital maneuvers using thrusters if necessary. On the other hand, rotational motion, or attitude motion, deals with the satellite's attitude around its center of mass separately from orbital motion. Attitude determination is done using on-board sensor instruments, while control is achieved through generating attitude control torques with on-board actuator instruments. The satellite's attitude is maintained in relation to a reference target attitude and/or rotational rate. The process of controlling spacecraft motion involves three main steps:

- Navigation which is Determining the current position and velocity of the satellite in its orbit, as well as the attitude and rotational rate of the satellite.
- Guidance which is Calculating the desired position and velocity of the target in orbit, along with the target's attitude and rotational rate, to achieve specific objectives.
- control which is Making adjustments to the satellite's position and velocity in orbit,

as well as its attitude and rotational rate, using actuators to maintain certain fixed values.

These steps, known as GNC (Guidance, Navigation, and Control), are carried out continuously and repeatedly. The accuracy of attitude control is dependent on the precision of each of these individual steps[**9**].

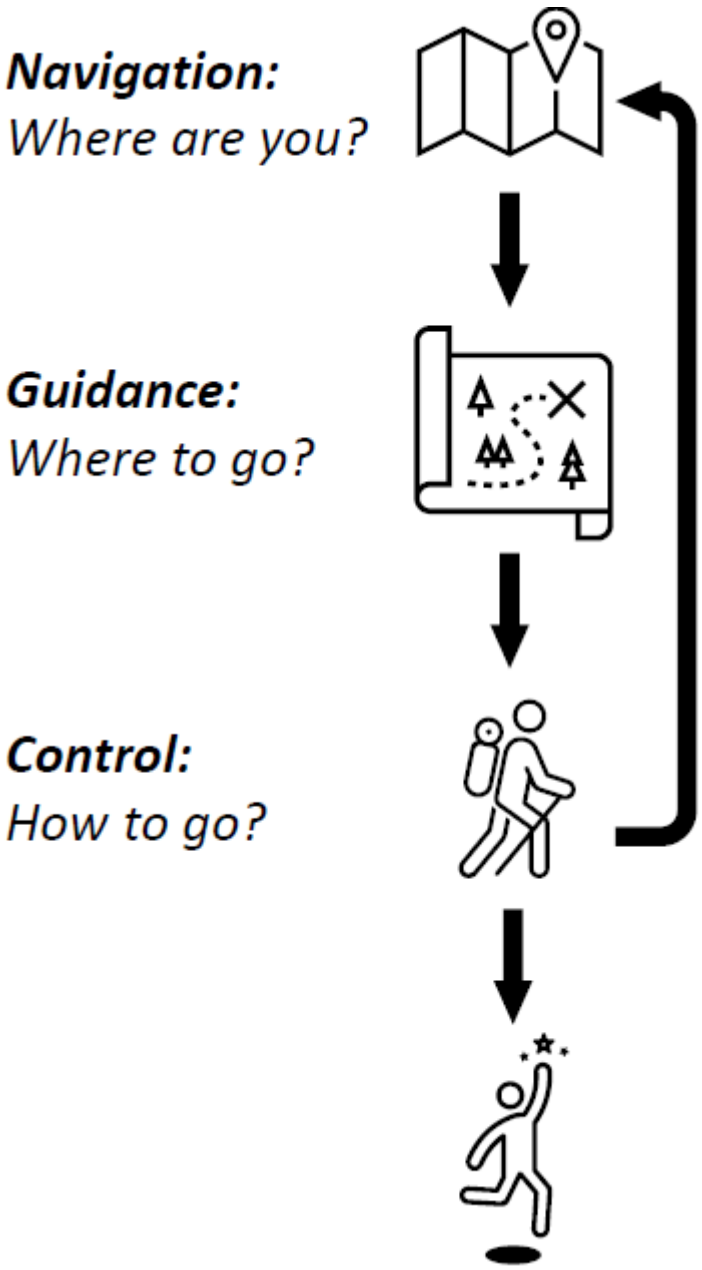

Figure 1.12: GNC (Guidance, Navigation, and Control)

Chapter 2

Advanced Dynamics and Control of Aerospace Systems

2.1 Dynamics for Systems of Particles

Newton's Second Law states that

$$\sum_{j=0}^{N} F_{ji} = \frac{dp_j}{dt} \tag{2.1}$$

where p_j is the momentum of a particle,

F_{ji} is a force on the particle.

Similar dynamic forumlations can be found in [**10**] , [**11**] , [**12**] , [**13**].

2.1.1 Rotational and Translational Dynamics for Systems of Particles

A system of particles rigidly connected can rotate about a center point. The center of mass of a system of particles can be defined using the relationship below:

$$r_C = \frac{1}{m} \sum_{j=0}^{P} m_j r_j \tag{2.2}$$

where

$$m = \sum_{j=0}^{P} m_j$$

To create rotational dynamics starting with the linear dynamics we use the equation below

$$M_C = \sum_{j=0}^{P} \mathbf{S}(r_{Cj}) \frac{dp_j}{dt} \tag{2.3}$$

P is the number of particles $\mathbf{S}(r_{Cj})$ is the skew symmetric matrix of the vector from the center of mass to the jth particle which results in a cross product. The skew symmetric operator is denoted by $S()$.

$$\mathbf{S}(r_{Cj}) = \begin{bmatrix} 0 & -z_{Cj} & y_{Cj} \\ z_{Cj} & 0 & -x_{Cj} \\ -y_{Cj} & x_{Cj} & 0 \end{bmatrix} \tag{2.4}$$

2.1.2 Rigid Bodies

many assumptions are made about the system of particles (Rigid Bodies).

1. The mass of each particle or rigid body is constant.

2. An inertial frame is placed at the center of the Earth that does not rotate with the Earth.

3. The rigid body is not flexible and does not change shape. That is, the time rate of change of the magnitude of a vector r_{PQ} is zero for any arbitrary points P and Q attached to the rigid body.

2.1.3 Translational Dynamics

For the Translational Dynamics, the momentum can be simplified to

$$\sum_{j=0}^{P} p_j = m v_{CI} \tag{2.5}$$

The derivation of the equation 2.5 starts by deriving the position of the center of mass as the following equation.

$$r_j = r_C + r_{Cj} \tag{2.6}$$

Taking one derivative results in the following equation

$$v_{jI} = v_{CI} + \frac{^{B}dr_{Cj}}{dt} + \mathbf{S}(\omega_{BI})r_{Cj} \tag{2.7}$$

Since the body is a rigid body the term $\frac{^{B}dr_{Cj}}{dt} = 0$

resulting in

$$v_{jI} = v_{CI} + \mathbf{S}(\omega_{BI})r_{Cj} \tag{2.8}$$

This equation can then be substituted into the equation for momentum such that.

$$\sum_{j=0}^{P} p_j = \sum_{j=0}^{P} m_j \left(v_{CI} + \mathbf{S}(\omega_{BI})r_{Cj}\right) \tag{2.9}$$

from the above equation we deduce the so called Newton-Euler equations of motion.

$$F_C = m\left(\frac{^{B}dv_{CI}}{dt} + \mathbf{S}(\omega_{BI})v_{CI}\right) \tag{2.10}$$

In Rotational Dynamics, a rigid body has

$$M_C = \frac{d}{dt}\sum_{j=0}^{P} \mathbf{S}(r_{Cj})m_j v_{jI} \tag{2.11}$$

Then the equation of two points fixed on a rigid body can be introduced to obtain the following equation

$$M_C = \frac{d}{dt}\sum_{j=0}^{P} \mathbf{S}(r_{Cj})m_j(v_{CI} + \mathbf{S}(\omega_{BI})r_{Cj}) \tag{2.12}$$

simplify this equation further yields

$$M_C = \frac{d}{dt}\left(\sum_{j=0}^{P} m_j \mathbf{S}(r_{Cj})\mathbf{S}(r_{Cj})^T \omega_{BI}\right) \tag{2.13}$$

The term in brackets is a well known value for rigid bodies and is known as the moment of inertia for rigid bodies.

$$I_C = \sum_{j=0}^{P} m_j \mathbf{S}(r_{Cj})\mathbf{S}(r_{Cj})^T \tag{2.14}$$

This results in the kinematic equations of motion for rigid bodies to the simple

equation below.

$$M_C = \frac{d}{dt}\left(I_C \omega_{BI}\right) \tag{2.15}$$

With the equation in this form it is possible to carry out the derivation to get

$$M_C = \frac{{}^B d(I_C \omega_{BI})}{dt} + \mathbf{S}(\omega_{BI}) I_C \omega_{BI} \dot{v} \tag{2.16}$$

the equation can simply be written as

$$M_C = \dot{I}\omega_{BI} + I_C \frac{{}^B d\omega_{BI}}{dt} + \mathbf{S}(\omega_{BI}) I_C \omega_{BI} \tag{2.17}$$

2.1.4 Inertia Estimation

There are several equations that can be used to compute the moment of inertia depending on the geometry of the vehicle. For this example we will look at a cuboid to demonstrate inertia calculations. Firstly, the total mass $mandsize(lengthl, widthw, andheighth)$ are required.

$$\begin{aligned} I_x &= \tfrac{m}{12}(l^2 + w^2) \\ I_x &= \tfrac{m}{12}(l^2 + w^2) \\ I_x &= \tfrac{m}{12}(l^2 + w^2) \end{aligned} \tag{2.18}$$

2.1.5 Aerospace Convention

using the Newton-Euler equations of motion to describe the vehicle, typically the position of the vehicle is written as

$$\mathbf{C}_I(r_C) = \begin{bmatrix} x \\ y \\ z \end{bmatrix} \tag{2.19}$$

The derivative of the position vector is the velocity vector is then written as

$$\mathbf{C}_I(v_{CI}) = \begin{bmatrix} \dot{x} \\ \dot{y} \\ \dot{z} \end{bmatrix} \tag{2.20}$$

In order to relate the body frame components of the velocity vector to the inertial frame coordinates, a transformation matrix is used to give the following equation.

$$\begin{bmatrix} \dot{x} \\ \dot{y} \\ \dot{z} \end{bmatrix} = T_{IB} \begin{bmatrix} u \\ v \\ w \end{bmatrix} \tag{2.21}$$

Standard aircraft/spacecraft forces and moments are applied to the body. The forces are typically written as X,Y and Z while the moments are given as L,M and N. They can be written in component form using the equations below. [1, 2, 3, 4].

$$\mathbf{C}_B(F_C) = \begin{bmatrix} X \\ Y \\ Z \end{bmatrix} = X\hat{I}_B + Y\hat{J}_B + Z\hat{K}_B \tag{2.22}$$

$$\mathbf{C}_B(M_C) = \begin{bmatrix} L \\ M \\ N \end{bmatrix} = L\hat{I}_B + M\hat{J}_B + N\hat{K}_B \tag{2.23}$$

2.1.6 Attitude Parameterization of Rigid Bodies

The matrix T_{IB} is a 3x3 transformation matrix that rotates a vector from the body to the inertial frame. A transformation matrix has the unique property that the inverse of the transformation is just the transpose of the matrix. There are multiple ways to construct this rotation frame:

Euler Angles

Euler angle are used to describe 3 unique rotation from the inertial to body frame. They are typically denoted as ψ, θ and ϕ. The order of the rotation can vary however the 3-2-1 sequence is standard for aircraft while the 3-1-3 sequence is standard for spacecraft.

(3-2-1) Sequence

The transformation from the inertial frame to the body frame involves three unique rotations. The first is a rotation about the z-axis such that

$$\mathbf{C}_A(v_{CI}) = [T_{IA}]^T \mathbf{C}_I(v_{CI}) = \begin{bmatrix} \cos\psi & \sin\psi & 0 \\ -\sin\psi & \cos\psi & 0 \\ 0 & 0 & 1 \end{bmatrix} \mathbf{C}_I(v_{CI}) \tag{2.24}$$

this rotation is called the yaw or heading rotation. From here the intermediate frame (A frame) is rotated about the y-axis such that

$$\mathbf{C}_{NR}(v_{CI}) = [T_{ANR}]^T \mathbf{C}_A(v_{CI}) = \begin{bmatrix} \cos\theta & 0 & -\sin\theta \\ 0 & 1 & 0 \\ \sin\theta & 0 & -\cos\theta \end{bmatrix} \mathbf{C}_A(v_{CI}) \tag{2.25}$$

this rotation is called the pitch angle rotation. Finally the (NR) no roll frame is rotated through the x-axis such that

$$\mathbf{C}_B(v_{CI}) = [T_{NRB}]^T \mathbf{C}_{NR}(v_{CI}) = \begin{bmatrix} 1 & 0 & 0 \\ 0 & \cos\phi & \sin\phi \\ 0 & -\sin\phi & \cos\phi \end{bmatrix} \mathbf{C}_{NR}(v_{CI}) \tag{2.26}$$

Putting all of these 2-D rotations together creates a transformation matrix from body to inertial.

$$\mathbf{C}_B(v_{CI}) = [T_{NRB}]^T [T_{ANR}]^T [T_{IA}]^T \mathbf{C}_I(v_{CI}) = [T_{IB}]^T \mathbf{C}_I(v_{CI}) \tag{2.27}$$

The inverse of this matrix is given below using the properties of matrix transposes. Standard shorthand notation is used for trigonometric functions: $\cos\alpha = c_\alpha, \sin\alpha = s_\alpha, and \tan\alpha = t_\alpha$.

$$\mathbf{T}_{BI}(\phi,\theta,\psi) = [T_{IA}][T_{ANR}][T_{NRB}] = \begin{bmatrix} c_\theta c_\psi & s_\phi s_\theta c_\psi - c_\phi s_\psi & c_\phi s_\theta c_\psi + s_\phi s_\psi \\ c_\theta s_\psi & s_\phi s_\theta s_\psi + c_\phi c_\psi & c_\phi s_\theta c_\psi - s_\phi c_\psi \\ -s_\theta & s_\phi c_\theta & c_\phi c_\theta \end{bmatrix} \tag{2.28}$$

Derivatives

If Euler angles are used to parameterize the orientation, the derivative of Euler angles is somewhat cumbersome to obtain. The angular velocity of a body is typically

written as

$$\omega_{BI} = \begin{bmatrix} p \\ q \\ r \end{bmatrix} = p\hat{I}_B + q\hat{J}_B + r\hat{K}_B \tag{2.29}$$

The angular velocity can be written in vector form such that

$$\omega_{BI} = \dot{\psi}\hat{K}_I + \dot{\theta}\hat{J}_{NR} + \dot{\phi}\hat{I}_B \tag{2.30}$$

relating the unit vectors $\hat{K}_I$ and $\hat{J}_{NR}$ to the body frame using the planar rotation matrices results in the equation below.

$$\begin{bmatrix} \dot{\phi} \\ \dot{\theta} \\ \dot{\psi} \end{bmatrix} = H \begin{bmatrix} p \\ q \\ r \end{bmatrix} \tag{2.31}$$

where H

$$H = \begin{bmatrix} 1 & s_\phi t_\theta & c_\phi t_\theta \\ 0 & c_\phi & -s_\phi \\ 0 & s_\phi c_\theta & c_\phi c_\theta \end{bmatrix} \tag{2.32}$$

Screw Rotation

It is often useful to extract Euler Angles from a unit vector. A unit vector has two degrees of freedom and thus has two rotations ψ and θ which can be determined using the equation below where $\hat{n}(1)$ denotes the first component of the vector in the body frame.

$$\psi = \tan^{-1}\left(\frac{\hat{n}(2)}{\hat{n}(1)}\right) \tag{2.33}$$

$$\theta = \tan^{-1}\left(\frac{\hat{n}(3)}{\hat{n}(1)^2 + \hat{n}(2)^2}\right) \tag{2.34}$$

Transformation Matrix to Euler Angles

Besides using unit vectors, sometimes it is beneficial to extract Euler angles from a known tranformation matrix. The equations below can be used to accomplish this where $T_{BI} = (T_{IB})^T$

$$\theta = -\sin^{-1} T_{BI}(1,3) \tag{2.35}$$

$$\phi = \tan^{-1} \frac{T_{BI}(2,3)}{T_{BI}(3,3)} \tag{2.36}$$

$$\psi = \tan^{-1} \frac{T_{BI}(1,2)}{T_{BI}(1,1)} \tag{2.37}$$

Quaternions

The orientation of the vehicle can be parameterized using four parameters known as quaternions Many supplemental equations and explanations can be found for quaternions in [**14**],[**15**],[**16**],[**17**],[**18**],[**19**],[**20**],[**21**].

$$q = \begin{bmatrix} q0 \\ q1 \\ q2 \\ q3 \end{bmatrix} \tag{2.38}$$

In this case 4 parameters are used to denote the quaternion. The rotation from the body to the inertial frame is the rotation of the inertial frame about the unit vector η through angle γ. The quaternion can then be written as

$$q = \begin{bmatrix} \cos(\gamma/2) \\ \eta \sin(\gamma/2) \end{bmatrix} \tag{2.39}$$

In this case it is possible to obtain the individual quaterions as $q0 = \cos(\gamma/2)$ and $\epsilon = [q1, q2, q3]^T = \eta \sin(\gamma/2)$ Furthermore, if given 4 quaternions, the angle γ is simply $\cos^{-1}(2q0)$ and $\eta = \frac{\epsilon}{\sin(\gamma/2)}$. Note that because a quaternion is essentially screw rotation about a known unit vector, there are two identical quaternions for every orientation.

Quaternion Transformations

In order to rotate the inertial frame to the body frame using quaternions, the transformation matrix is shown below.

$$T_{BI}(q) = \begin{bmatrix} q0^2 + q1^2 - q2^2 - q3^2 & 2(q1q2 + q0q3) & 2(q1q3 - q0q2) \\ 2(q1q2 - q0q3) & q0^2 - q1^2 + q2^2 - q3^2 & 2(q0q1 + q2q3) \\ 2(q0q2 - q1q3) & 2(q2q3 - q0q1 & q0^2 - q1^2 - q2^2 + q3^2 \end{bmatrix} \tag{2.40}$$

Euler to Quaternion Transformations

converting quaternions to Euler angles is a standard operation and shown below

$$\phi = \tan^{-1}\left(\frac{2(q0q1 + q2q3)}{1 - 2(q1^2 + q2^2)}\right) \tag{2.41}$$

$$\theta = \sin^{-1}\left(2(q0q2 - q3q1)\right) \tag{2.42}$$

$$\psi = \tan^{-1}\left(\frac{2(q0q3 + q1q2)}{1 - 2(q2^2 + q3^2)}\right) \tag{2.43}$$

It is also possible to convert Euler angles to quaternions using the equations below.

$$\begin{aligned} q0 &= \cos(\phi/2)\cos(\theta/2)\cos(\psi/2) + \sin(\phi/2)\sin(\theta/2)\sin(\psi/2) \\ q1 &= \sin(\phi/2)\cos(\theta/2)\cos(\psi/2) - \cos(\phi/2)\sin(\theta/2)\sin(\psi/2) \\ q2 &= \cos(\phi/2)\sin(\theta/2)\cos(\psi/2) + \sin(\phi/2)\cos(\theta/2)\sin(\psi/2) \\ q3 &= \cos(\phi/2)\cos(\theta/2)\sin(\psi/2) - \sin(\phi/2)\sin(\theta/2)\cos(\psi/2) \end{aligned} \tag{2.44}$$

Quaternion Operations

The norm of the quaternions is given by $|q| = \sqrt{q0^2 + q1^2 + q2^2 + q3^2}$. In standard spacecraft applications, the norm of the quaternion is just 1. The conjugate of

the quaternion is given below.

$$q^* = \begin{bmatrix} q0 \\ -q1 \\ -q2 \\ -q3 \end{bmatrix} \tag{2.45}$$

Quaternion Derivatives

The derivatives of a quaternion are written in shorthand using the equation below.

$$\dot{q} = \frac{1}{2}\Omega(\omega_{BI})q \tag{2.46}$$

These vector operators can then be used to expand the kinematic derivatives as shown by equation below

$$\begin{bmatrix} \dot{q}0 \\ \dot{q}1 \\ \dot{q}2 \\ \dot{q}3 \end{bmatrix} = \frac{1}{2}\begin{bmatrix} 0 & -p & -q & -r \\ p & 0 & r & -q \\ q & -r & 0 & p \\ r & q & -p & 0 \end{bmatrix}\begin{bmatrix} q0 \\ q1 \\ q2 \\ q3 \end{bmatrix} \tag{2.47}$$

where qi are the four quaternions and p, q, r are the components of the angular velocity vector in the body frame.

2.2 Aerospace Equations of Motion

2.2.1 Translational Equations of Motion

The translational equations of motion of satellites are fairly simple given that everything is written in the inertial frame. The position vector of the vehicle is $r = [x, y, z]^T$ and the velocity is $v_{BI} = [\dot{x}, \dot{y}, \dot{z}]^T$. The acceleration of the vehicle is found by summing the total forces on the body and dividing by the mass of the vehicle. In the equation below $N_\oplus$ is the number of planetary bodies acting on the vehicle while F_P is the force imparted by thrusters.

$$\alpha_{BI} = \frac{1}{m_s}\left(\sum_{i=1}^{N_\oplus} F_i + F_P\right) \tag{2.48}$$

Note that for a spacecraft the magnitude of the gravitational acceleration vector is on the order of $\pm 10 m/s^2$. Sources point to solar radiation pressure being on the order of $4.5 \mu Pa$ [**22**]. For a 1U CubeSat (10 cm x 10 cm) the force would be equal to $0.45 mN$. A 1U CubeSat has a nominal mass of 1 kg which would accelerate the CubeSat on the order of $0.45 mm/s^2$, which is considerably less than gravitational acceleration. Furthermore, using the standard aerodynamic drag equation ($0.5 \rho V^2 S C_D$), where conservative estimates are used, the aerodynamic force at 600 km above the Earth's surface would be about $3.0 \eta N$ [**23**]. This assumes a density equal to $1.03 \times 10^{-14} kg/m^3$, a velocity equal to $7.56 km/s$, and a drag coefficient equal to 1.0 [**24**]. A force this small would impart an acceleration of about $3.0 \eta m/s^2$ which is also considerably less than gravitational acceleration. These forces cannot be neglected for longer missions but can be ignored where appropriate. For an aircraft and quadcopter the equations of motion are typically written in the body frame. As such the derivative transport theorem is used and the translational equations of motion are written as the following:

$$\begin{bmatrix} \dot{u} \\ \dot{v} \\ \dot{w} \end{bmatrix} = \frac{1}{m} \begin{bmatrix} X \\ Y \\ Z \end{bmatrix} - \begin{bmatrix} 0 & -r & q \\ r & 0 & -p \\ -q & p & 0 \end{bmatrix} \begin{bmatrix} u \\ v \\ w \end{bmatrix} \tag{2.49}$$

2.2.2 Reaction Wheel Model

The reaction wheel model must be included before the attitude dynamics because they directly affect the inertia of the vehicle. There are three reaction wheels on this vehicle and each one has it's own angular velocity ω_{Ri} and angular acceleration α_{Ri} . The inertia of each reaction wheel is first written about the center of mass of the reaction wheel and is given by the equation below where the reaction wheel is modeled as a disk with finite radius r_{RW} and height h_{RW}. The subscript R is used to denote that this inertia matrix is about the center of mass of the reaction wheel while the super script R is used to denote the frame of reference.

$$I_{Ri}^{R} = \begin{bmatrix} \frac{m_R r_{RW}^2}{2} & 0 & 0 \\ 0 & \frac{m_R}{12}(3r_{RW}^2 + h_{RW}^2) & 0 \\ 0 & 0 & \frac{m_R}{12}(3r_{RW}^2 + h_{RW}^2) \end{bmatrix} \tag{2.50}$$

In order to rotate the inertia matrix into the vehicle body frame of reference an

axis of reaction wheel rotation is used. The vector n_{Ri} is used to denote the axis about which the reaction wheel rotates. Euler Angles θ_{Ri} and ϕ_{Ri} can be extracted from this unit vector as discussed previously. The rotation matrix $T_{Ri}(0, \theta_{Ri}, \psi Ri)$ can then be generated using equation 2.28. This matrix can then be used to compute the inertia of the reaction wheel in the vehicle body frame

$$I_{Ri}^{B} = T_{Ri} I_{Ri}^{R} \tag{2.51}$$

The parallel axis theorem can then be used to shift the inertias to the center of mass of the vehicle where the subscript RB denotes the reaction wheel inertia taken about the center of mass of the vehicle.

$$I_{RBi}^{B} = I_{Ri}^{B} + m_{Ri}\mathbf{S}(r_{Ri})\mathbf{S}(r_{Ri})^{T} \tag{2.52}$$

The vector $r_{Ri}$is the distance from the center of mass of the vehicle to the center of mass of the reaction wheel in the vehicle body reference frame. The total inertia of the entire vehicle-reaction wheel system is then just a sum of all the reaction wheel inertias.

$$I_S = I_B + \sum_{i=1}^{3} I_{Ri}^{B} \tag{2.53}$$

The total angular momentum of the vehicle is then equal to the following equation where ω_{BI} is the angular velocity of the vehicle.

$$H_S = I_B \omega_{BI} + \sum_{i=1}^{3} I_{Ri}^{B} \omega_{Ri} n_{Ri} \tag{2.54}$$

In a similar fashion, the total torque placed on the vehicle is equal to the following

$$M_R = \sum_{i=1}^{3} I_{Ri}^{B} \alpha_{Ri} n_{Ri} \tag{2.55}$$

It is typically assumed that the angular acceleration of each reaction wheel can be directly controlled. However, as the reaction wheel angular velocity increases, the maximum angular acceleration allowed begins to decrease. Once the reaction wheel reaches its angular velocity limits, the angular acceleration possible drops to zero. This is called reaction wheel saturation and must be dealt with using a method called

momentum dumping.

2.2.3 Attitude Equations of Motion

The attitude equations of motion are formulated assuming the vehicle can rotate about three axes. The derivative of angular velocity is found by equating the derivative of angular momentum to the total moments placed on the vehicle while reaction wheel torques from the vehicle are added.

$$\dot{\omega}_{BI} = I_S^{-1}(M_P + M_M + M_R - S(\omega_{BI})H_S - \dot{I}_S\omega_{BI}) \tag{2.56}$$

The applied moments use subscripts P for propulsion, M for magnetorquers, and R for reaction wheels. The term $\dot{I}_S$ is the change in inertia in the body frame caused by deployment of solar panels and/or antenna. Also, recall that H_S is the total angular momentum of the entire vehicle including the reaction wheels if present. For aircraft the rotational dynamic equation can be found as

$$\begin{bmatrix} \dot{p} \\ \dot{q} \\ \dot{r} \end{bmatrix} = I_C^{-1} \left(\begin{bmatrix} L \\ M \\ N \end{bmatrix} - \begin{bmatrix} 0 & -r & q \\ r & 0 & -p \\ -q & p & 0 \end{bmatrix} I_C \begin{bmatrix} p \\ q \\ r \end{bmatrix} \right) \tag{2.57}$$

2.3 External Models

Many external models are used in simulation to accurately depict the environment. The magnetic field model comes from the Geographic Library model which uses the EMM2015 magnetic field model. The gravitational model comes from the EGM2008 model[**25**].

2.3.1 GPS Coordinates to Cartesian Coordinates

it is useful to convert the GPS coordinates (latitude,longitude, altitude,($\lambda_{Lat}, \lambda_{Long}, h$) to a flat earth approximation where the x-axis is pointing North, the y-axis is pointing east and the z-axis is pointing towards the center of the planet. The equations to convert LLH (latitude,longitude, altitude) to a cartesian coordinate system are given below. Note that these equations assume that the vehicle creates an origin point to

define as the center of the inertial frame which is on the surface of the planet rather than the center of the planet $\lambda_{Lat,0}, \lambda_{Long,0}$

$$\begin{aligned} x &= k(\lambda_{Lat} - \lambda_{Lat,0}) \\ y &= k(\lambda_{Long} - \lambda_{Long,0})\cos(\tfrac{\pi\lambda_{Lat}}{180}) \\ z &= -h \end{aligned} \tag{2.58}$$

2.3.2 Density Model

The density model is simply given as an exponential model.

$$\rho = \rho_s e^{-\sigma h} \tag{2.59}$$

where ρ_s is the density at sea-level, h is the altitude above the Earth in kilometers and $\sigma = 0.1354 km^{-1}$ is known as the scale height [**26**] , [**27**] , [**28**]

2.3.3 Magnetic Field Model

The Magnetic Field model used in this simulation stems from the Enhanced Magnetic Field Model (EMM2015) [**29**].

Specifically, the inputs to the model are the position x, y, z of the satellite assuming an inertial frame with the z-axis pointing through the north pole and the x axis pointing through the equator at the prime meridian . This is known as the Earth-Centered Inertial (ECI) coordinate system .

In order to connect these inertial coordinates (x, y, z) to be used in the EMM2015 model, the latitude, longitude and height above the surface of the Earth are required. To do this, the coordinates are converted into spherical coordinates using the equations below.

$$\begin{aligned} \rho &= \sqrt{x^2 + y^2 + z^2} \\ \phi_E &= 0 \\ \theta_E &= \cos^{-1}(\tfrac{z}{\rho}) \\ \psi_E &= \tan^{-1}(\tfrac{y}{x}) \end{aligned} \tag{2.60}$$

Note that $\rho, \phi_E, \theta_E, \psi_E$ are related to latitude and longitude coordinates but not

quite the same. In order to obtain the latitude and longitude coordinates the following equations are used. The height is simply the distance from the center of the ECI frame minus the reference height from the approximation of Earth as an ellipsoid ($R_{\oplus} = 6,371,393 meters$). Note that the angles from Equation 2.64 are converted to degrees.

$$\begin{aligned} \lambda_{Lat} &= 90 - \theta_E \tfrac{180}{\pi} \\ \lambda_{Long} &= \psi_E \tfrac{180}{\pi} \\ h &= \rho - R_{\oplus} \end{aligned} \tag{2.61}$$

The inputs to the EMM2015 model are the latitude, longitude and height. The inverse of the above two equations are given below. These would be used in the event a latitude and longitude coordinate is given and there is a need to obtain the x,y and z coordinates in the ECI frame. The first step is to convert latitude, longitude and altitude and convert that to standard spherical angles and distance from the center of the planet.

$$\begin{aligned} \theta_E &= (90 - \lambda_{Lat}) \tfrac{\pi}{180} \\ \psi_E &= (\lambda_{Long}) \tfrac{\pi}{180} \\ \rho &= h + R_{\oplus} \end{aligned} \tag{2.62}$$

Once that is complete the extraction of x,y and z are computed by the equation below.

$$\begin{aligned} x &= \rho \sin\theta_E \cos\psi_E \\ y &= \rho \sin\theta_E \sin\psi_E \\ z &= \rho \cos\theta_E \end{aligned} \tag{2.63}$$

The output from the EMM2015 model is in the East, North, Vertical (ENV) reference frame where the x-axis is East pointing in the direction of the rotation on the Earth, the y-axis is North pointing towards the North pole and finally the z-axis is the Vertical component that is always pointing radially away from the center of the Earth. In order to get the coordinates into the ECI frame the coordinates must first be converted to the North, East, Down reference frame (NED). In this case the x-axis is pointing North, the y-axis pointing East and the z-axis is always pointing towards the center of the Earth and called Down. The equation to rotate from the ENV frame

to NED frame is shown below.

$$\begin{bmatrix} \beta_x \\ \beta_y \\ \beta_z \end{bmatrix}_{NED} = \begin{bmatrix} 0 & 1 & 0 \\ 1 & 0 & 0 \\ 0 & 0 & -1 \end{bmatrix} \begin{bmatrix} \beta_x \\ \beta_y \\ \beta_z \end{bmatrix}_{ENV} \tag{2.64}$$

Once the magnetic field is in the NED reference frame it can then be rotated to the inertial frame using the following equation where β_{NED} is the magnetic field in the NED coordinate system and β_I is the magnetic field in the inertial frame.

$$\beta_I = T_{IB}(0, \theta_E + \pi, \psi_E)\beta_{NED} \tag{2.65}$$

The matrix $T_{IB}(\phi, \theta, \psi)$ represents the transformation matrix from the spherical reference frame to the inertial reference frame. Note that there is no rotation about the x-axis through ϕ and the pitch rotation is augmented by π because of the switch between North, East, Down (NED) and the z-axis of the ECI pointing through the North pole. The result of these equations, is the ability to obtain the magnetic field across an entire orbit.

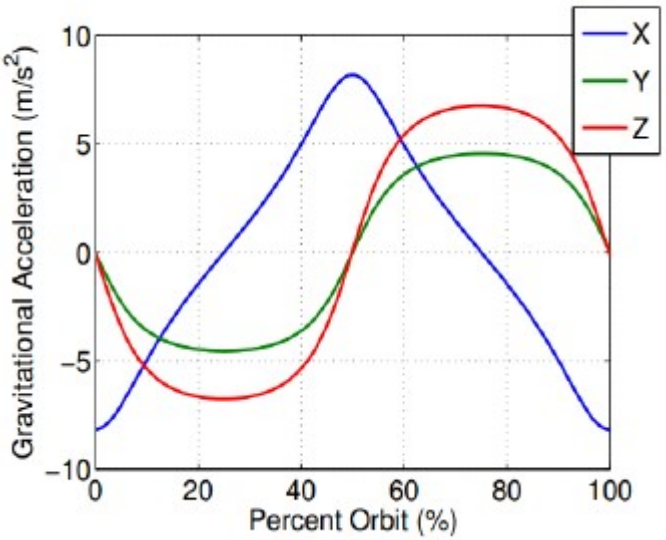

Figure 2.1: Gravitational Field of Earth in Inertial Frame for 56 Degree Orbit at 600 km Above Surface

2.3.4 Gravitational Models

The the gravitational field vector is

$$F_{\oplus} = \frac{m_{\oplus} m_s}{r^2} \tag{2.66}$$

The gravitational field model stems from the Earth Gravity Model (EGM2008) [**30**] , figure 2.1 shows Gravitational Field of Earth in Inertial Frame for 56 Degree Orbit at 600km Above Surface

2.3.5 External Forces and Moments

In addition to gravity acting on a vehicle, other forces also act on the satellite. For a 1U CubeSat, the gravity gradient over 10 cm is about $0.24 \mu m/s^2$ using the EGM2008 model. Multiplying this acceleration by a 1 kg mass and applying a 10 cm moment arm yields a moment of about $2.4 \times 10^{-8} Nm$. Aerodynamic torques could be as large as $1.5 \times 10^{-10} Nm$ assuming the aerodynamic center is 5 cm away from the center of mass. Typical magnetorquers operate in the vicinity of $3.0 \times 10^{-6} Nm$, assuming a current of $0.04A$, an area of $0.02m^2$, 84 turns and a magnetic field of $40,000 \eta T$. Using these calculations, magnetorquers are two orders of magnitude larger than gravity torques and four orders of magnitude larger than aerodynamic torques. It is important to keep these values in mind when neglecting certain parameters [**31**],[**32**],[**33**].

2.3.6 Solar Radiation Pressure

Solar radiation pressure is relatively constant at 1 AU and thus is simply given as $ps = 4.5e - 6Pa$. The force is then found to be just the pressure multiplied by the frontal area of the satellite. The torque, is the force crossed with a distance vector from the center of mass to the center of pressure of solar radiation. The vector $\hat{s}$ is a unit vector denoting the direction of the sun.

$$F_{SR} = P_s S \hat{s} \tag{2.67}$$

$$M_{SR} = \mathbf{S}(F_{SR}) r_{CG-CP_s} \tag{2.68}$$

2.3.7 Magnetorquer Model

The magnetorquer model assumes that three magnetorquers are aligned in such a way that the magnetic moment produced by each magnetorquer is aligned with the principal axes of the body frame of the satellite. Each magnetorquer is controlled independently such that$i_M = [i_x, i_y, i_z]^T$ which is the applied current in each magnetorquer. The magnetic moment is then given by the equation below

$$\mu_M = \eta A i_M \tag{2.69}$$

where η is the number of turns in the coil of each magnetorquer and A is the area of the magnetorquer. For simplicity it is assumed that all magnetorquers have the same area and same number of turns. The torque produced by all magnetorquers is then simply found by crossing the magnetic moment with the magnetic field of the Earth in the Body reference frame.

$$M_M = \mathbf{S}(\mu_M) T_{BI}(q) \beta_I \tag{2.70}$$

In order to obtain the magnetic field vector in the body frame, the inertial magnetic field vector must be rotated into the body frame of the satellite. In component form, equation (2.69) reduces to the following equation using the identity that $a \times b = -b \times a$

$$\begin{bmatrix} L_M \\ M_M \\ N_M \end{bmatrix} = \eta A \begin{bmatrix} 0 & \beta_z & -\beta_y \\ -beta_z & 0 & \beta_x \\ \beta_y & -\beta_x & 0 \end{bmatrix} \begin{bmatrix} i_x \\ i_y \\ i_z \end{bmatrix} \tag{2.71}$$

where $\beta_x, \beta_y, \beta_z$ are the components of the magnetic field in the body frame of the satellite. The moments L, M, N are thus the control torques that rotate the satellite as seen in equation (2.57).

2.3.8 Spacecraft Aerodynamics

The aerodynamic force is computed using aerodynamic coefficients and dynamic pressure where$V$ is the velocity of the satellite and V is the magnitude of the velocity vector. Furthermore, S is the surface area of the satellite and C_D is the drag coefficient. The torque on the satellite is then given by the cross product between the aerodynamic

force and a distance vector representing the distance between the center of mass and the center of pressure r_{CP-CG}.

$$F_A = \frac{1}{2}\rho V V S C_D \tag{2.72}$$

$$M_A = -\mathbf{S}(F_A) r_{CP-CG} \tag{2.73}$$

2.4 Guidance Navigation and Controls

Every vehicle must be able to maintain a specific position within its flight or orbit as well as point in a specific direction to achieve its mission. Mission goals have specific trajectories or orbits that must be reached and maintained, and this section is intended to explain how this is done from a guidance navigation and controls perspective. The basis for the guidance, navigation, and control (GNC) subsystem are attitude control, attitude estimation, and position estimation. Attitude describes which direction the vehicle is pointing in three-dimensional space. Attitude control is the act of controlling the orientation of the vehicle while attitude estimation is the process of determining the precise direction of the vehicle in order to perform attitude control. Position estimation primarily involves integration schemes or GPS in order to determine the position of the vehicle on the surface of the planet. While performing the mission, the vehicle will continually use this subsystem to document the position. The basis of these techniques follows an understanding of spaceflight mechanics and systems engineering.

The GNC subsystem is critical for the survival of the vehicle. It is the system that determines the vehicles orientation and position in space. Guidance is task of computing the desired trajectory and orientation of a vehicle. Guidance is completed by using components to determine any changes in position, altitude, or orientation to assist the vehicle in following its projected trajectory. Similar to guidance, navigation is the system's way of leading the vehicle in space and keeping it on its intended path.

In order to have a successful flight and achieve the intended mission goal the vehicle needs to be stable and controlled in space. There are many different components different aerospace vehicles use to accomplish this. Satellites use reaction wheels and gimbaled thrusters to name a few while aircraft use aerodynamic surfaces.

2.4.1 Vehicle State Estimation

Vehicle State estimation is a fundamental portion of GNC and requires the vehicle to determine it's orientation with respect to an inertial frame as well as its position from an inertial reference point. Some sensors are specific to the vehicle application but here this section will discuss a standard INS (Inertial Navigation System) which consists of a GPS (Global Positioning System) and an IMU (Inertial Measurement Unit).

Inertial Measurement Unit

An inertial measurement unit (IMU) is a combination of three sensors. An accelerometer, rate gyro and magnetometer. A magnetometer is a device that measures the local magnetic field in the body frame $\hat{\beta}_B = [\hat{\beta}_x, \hat{\beta}_y, \hat{\beta}_z]^T$ **[34]**. Note that the ˆimplies a measurement rather than the truth signal. Measurements from sensors are prone to bias, drift, scale factor, misalignment, noise and other sources of error that must be accounted for.

A rate gyroscope, commonly referred to as a rate gyro measures the angular velocity also in the body frame

$$\hat{\omega}_{BI} = [\hat{g}_x, \hat{g}_y, \hat{g}_z]^T \tag{2.74}$$

Accelerometers are sensors used to measure acceleration at a point P on a rigid body ˆaBI $\hat{a}_{BI} = [\hat{a}_x, \hat{a}_y, \hat{a}_z]^T$. For simplicity however, it is assumed that point P on the rigid body is the center of mass point C therefore the accelerometer is measuring the acceleration of the body itself in the body frame with respect to an inertial frame BI

As mentioned before, the IMU consists of 3 sensors all returning 3 measurments. This results in 9 scalar quantities being returned from this sensor which is where the term 9DOF gets it origin In reality DOF means Degrees of Freedom which is contrary to the standard 6DOF simulation models explained above. However, the sensor community chooses to coin the term 9DOF to highlight the 9 different scalar values returned from IMUs. It is possible to obtain a 10DOF sensor which also returns pressure or temperature data.

2.4.2 Euler Angle Estimation via IMU

Using an IMU it is possible to obtain Euler Angles assuming a Flat Earth Approximation. Recall that Euler angles are a 3D transformation from the Inertial frame to the Body Frame . The angle ϕ and θ can directly be measured via the accelerometer by creating a relationship between the gravity vector in the inertial and body frames. The heading angle can be measured by creating a relationship between the magnetic field in the body frame and the inertial frame using a magnetometer. The rate gyro can be used to integrate the angular velocity to obtain Euler angles as well but is prone to drift. The accelerometer though is prone to errors when the vehicle experiences large acceleration loads. Thus, typically the Euler angles from the rate gyro are fused with the estimates from the magnetometer and the accelerometer.

2.4.3 Low Earth Orbit Attitude Estimation

In LEO the main algorithm begins with obtaining the magnetic field in the body frame using magnetometers β_B. Using the IGRF model the locally measured magnetic field can be compared with the known magnetic field for any given location within its orbit. Using the true data and the measured data, the spacecraft can compute its actual position to the measured position and make the correct adjustments. A Sun measurement is then taken using a Sun sensor $\S_B$.. Once those two independent body frame measurements are taken the inertial reference vectors must be obtained from a database. Startrackers have this database built in; however, for the magnetic field and the Sun vector these must be obtained from a separate database. The idea is that if the position of the Earth is known then the position of the Sun with respect to the Earth is also known. The magnetic field vector can be obtained from the IGRF model. The magnetic field vector in the inertial frame is given as β_I.. Note that the IGRF model requires the latitude and longitude to be known. Thus, in LEO a GPS is required to feed into the database. The inertial Sun vector $\S_I$ only requires the Julian time which can be obtained from GPS as well. The julian time is based on the julian day. The initial attitude determination algorithm itself requires two independent vectors. As stated previously, startrackers provided a large enough aperture and enough stars to produce the full quaternion by obtaining multiple unique vectors to unique stars. Multiple solar sensors or multiple magnetometers unfortunately do not obtain non-

unique vectors and the algorithm fails. In LEO this is typically done with solar sensors and magnetometers but it can be done with star trackers. In deep space it is typically done with startrackers but it could be possible to obtain a Moon vector that would require a Moon sensor. The derivation below is done for the LEO case with a Sun and magnetic field measurement. The derivation is identical for the deep space case with a Moon sensor simply by substituting the magnetic field measurment with a Moon measurement. Every vector is first normalized to obtain β_B, β_I $\S_B$, $\S_I$. A triad is then created from body frame vectors using the equations below.

$$\hat{f}_1 = \hat{S}_B,\ \hat{f}_2 = \hat{f}_1 \times \hat{\beta}_B,\ \hat{f}_3 = \hat{f}_1 \times \hat{f}_2, \tag{2.75}$$

The matrix **F** is then created using the triad as an orthonormal basis $F = [\hat{f}_1, \hat{f}_2, \hat{f}_3]$. Similar equations are used for the inertial measurements.

$$\hat{g}_1 = \hat{S}_I,\ \hat{g}_2 = \hat{g}_1 \times \hat{\beta}_I,\ \hat{g}_3 = \hat{g}_1 \times \hat{g}_2, \tag{2.76}$$

The matrix **G** is then created just as the F matrix such that $G = [\hat{g}_1, \hat{g}_2, \hat{g}_3]$. The transformation from inertial to body frame is then created using the formula below.

$$T_{BI} = FG^T \tag{2.77}$$

This matrix above is similar to the matrix in equation 2.28 and thus the Euler angles can be extracted from the matrix itself using the formulation defined in Section 'Attitude Parameterization of Rigid Bodies'. Euler can then be converted to quaternions if needed. Note that it is relatively easy to extract Euler angles from the TIB matrix, it is not so simple to extract quaternions. This is due to the fact that for every orientation there exists two quaternions that represent this space. Thus, it is more ideal to obtain Euler angles from the transformation matrix and then convert them to quaternions.

2.5 Spacecraft Attitude Control Schemes

Many control schemes are needed to orient a satellite and all depend on the application. In LEO magnetorquers can be used to detumble a satellite while thrusters

must be used in deep space. In addition reaction wheels can be used to detumble a satellite anywhere in space provided the angular momentum in the satellite does not saturate the reaction wheels.

2.5.1 B-dot Controller

In LEO, the standard B-dot controller reported in many sources [**35**],[**36**],[**37**],[**38**] can be used to de-tumble a satellite. The standard B-dot controller requires the magnetorquers to follow the control law shown below

$$\mu_B = k\mathbf{S}(\omega_{BI})T_{BI}(q)\beta_I \tag{2.78}$$

where k is the control gain. Using equation (2.71) it is possible to write the current in component form again using the identity that $a \times b = -b \times a$

$$\begin{bmatrix} i_x \\ i_y \\ i_z \end{bmatrix} = \frac{k}{\eta A} \begin{bmatrix} 0 & \beta_z & -\beta_y \\ -\beta_z & 0 & \beta_x \\ \beta_y & -\beta_x & 0 \end{bmatrix} \begin{bmatrix} p \\ q \\ r \end{bmatrix} \tag{2.79}$$

This equation can then be substituted into equation (2.71) to produce the total torque on the satellite assuming that the magnetorquers can provide the necessary current commanded by equation (2.80).

$$\begin{bmatrix} L \\ M \\ N \end{bmatrix} = -K \begin{bmatrix} \beta_y^2 + \beta_z^2 & -\beta_x\beta_y & -\beta_x\beta_z \\ -\beta_x\beta_y & \beta_x^2 + \beta_z^2 & -\beta_y\beta_z \\ -\beta_x\beta_z & -\beta_y\beta_z & \beta_x^2 + \beta_y^2 \end{bmatrix} \begin{bmatrix} p \\ q \\ r \end{bmatrix} \tag{2.80}$$

The goal of the controller here is to drive $\omega_{BI} \to 0$. The literature will show that this is not completely achieved [**46**]. There are multiple explanations for this. For starters, equation (2.70) assumes that the magnetic moment is not co-linear with the magnetic field of the Earth. If it is, the result is zero torque applied to the satellite. Furthermore, equation (2.80) results in zero current if the angular velocity vector of the satellite is co-linear with the magnetic field. Thus, if the magnetic field vector, angular velocity vector or the magnetic moment vector are co-linear, the torque applied to the satellite will be zero. If a new operator is defined such that

$$W(T_{BI}(q)\beta_I) = \begin{bmatrix} \beta_y^2 + \beta_z^2 & -\beta_x\beta_y & -\beta_x\beta_z \\ -\beta_x\beta_y & \beta_x^2 + \beta_z^2 & -\beta_y\beta_z \\ -\beta_x\beta_z & -\beta_y\beta_z & \beta_x^2 + \beta_y^2 \end{bmatrix} \tag{2.81}$$

it is easy to see that the torque applied to a satellite is then simply the angular velocity vector multiplied by this transition matrix. If this transition matrix is put into row-reduced-echelon form it is easy to see that the determinant of this matrix is equal to zero .

$$rref(W(T_{BI}(q)\beta_I)) = \begin{bmatrix} 0 & 1 & -\beta_x/\beta_z \\ 0 & 1 & -\beta_y/\beta_z \\ 0 & 0 & 0 \end{bmatrix} \tag{2.82}$$

A zero determinant means that there exists a vector ω_{BI} that will result in zero torque for a given value of the magnetic field. This is typically avoided since the magnetic field of the Earth is time and spatially varying which results in a transition matrix that changes over time due to orientation changes in the satellite as well as changes in the satellite's orbit. However, for low inclination orbits, it's possible for the magnetic field to stay relatively constant with $\beta_x = \beta_y = 0$. If the satellite is tumbling about the yaw axis such that $p = q = 0$, the yaw torque on the satellite (N) will be zero. Using this simple controller, there is no way to remove the remaining angular velocity from the satellite unless reaction wheels are used.

2.5.2 Reaction Wheel Control

Assuming each reaction is aligned with a principal axis of inertia the control scheme is extremely simple. When the wheels are not aligned the derivation will proceed similar to the reaction control thruster section. The derivation here will just be for the aligned case. In this analysis it is assumed that a torque can be applied to the reaction wheel and thus the angular velocity of the reaction wheel α_{Ri} can be directly controlled. Assuming this a simple PD control law can be used to orient the satellite at any desired orientation using Euler angles for this control law since the satellites are aligned with the principal axes of rotation .

$$\alpha_{Ri} = -k_p(\epsilon_i - \epsilon_{desired}) - k_d(\omega - \omega_{desired}) \tag{2.83}$$

In the equation above ϵ denotes either roll ϕ, pitch θ or yaw ψ depending on which reaction wheel is being used. The Euler angles in this case would be obtained by converting the quaternions to Euler angles.

Often times however your reaction wheels are not pointed on the principal axis of inertia. In this case a Least Squares Regression model is needed. In this case the equation above is used to compute the desired torque to be placed on the satellite such that

$$M_{desired} = -k_p(\epsilon_i - \epsilon_{desired}) - k_d(\omega - \omega_{desired}) \tag{2.84}$$

This equation is then equated to the equation for torque placed on the satellite where the angular accelerations are placed into a vector.

$$M_{desired} = M_R = \sum_{i=1}^{NR} I^B_{Ri}\alpha_{Ri}\hat{n}_{Ri} = [I^B_{Ri}\hat{n}_{Ri} \dots I^B_{RNR}\hat{n}_{RNR}] \begin{bmatrix} \alpha_1 \\ .... \\ \alpha_{NR} \end{bmatrix} = J\alpha \tag{2.85}$$

Since J is a $3 \times N_{RW}$ matrix its impossible to simply invert the matrix and solve for the vector of angular accelerations α. In this case there are an infinite number of solutions. As such a minimization routine is required where the solution found also happens to be the lowest amount of angular acceleration. In this case, Lagrange's method was used to find the vector of angular accelerations[**39**] .

$$\alpha = J^T(JJ^T)^{-1}M_{measured} \tag{2.86}$$

Chapter 3

Simulation and Analysis

Attitude Determination and Control (ADC) is a crucial subsystem in the operation of CubeSats, ensuring that these small satellites can achieve and maintain the desired orientation in space. Precise control of a CubeSat's attitude is essential for mission objectives such as Earth observation, communication, and scientific experiments. This section outlines the procedures undertaken to simulate the ADC system for CubeSats utilizing reaction wheels, which provide the necessary torques for attitude adjustments without expelling mass.

The simulation aims to validate the performance of control algorithms and the integration of hardware components under various operating conditions. By accurately modeling the dynamics of the CubeSat and the behavior of the reaction wheels, we can predict the system's response to control inputs and external disturbances. This process involves the development of mathematical models, implementation of control strategies, and execution of simulation scenarios that replicate real-world conditions.

The procedures detailed herein encompass the entire simulation workflow, from the initial system modeling to the analysis of simulation results. This comprehensive approach ensures that all aspects of the ADC system are thoroughly tested and validated, providing valuable insights into the feasibility and effectiveness of the proposed design for CubeSat missions.

3.1 Simulation Environment

Initial Conditions Position and Velocity

The Initial Conditions Position and Velocity velocity of the CubeSat were carefully chosen to represent realistic scenarios encountered in orbit.

altitude = 600*1000 (meters)

x0 = R + altitude

y0 = 0

z0 = 0

inclination = 56*pi/180

semi major axis= norm([x0;y0;z0])

vcircular = sqrt(mu/semi major)

$\dot{x}0$ =0

$\dot{y}0$= vcircular*cos(inclination)

$\dot{z}0$ = vcircular*sin(inclination)

period = 2*pi/sqrt(mu)*$(semi\ major\ axis)^{\frac{3}{2}}$

number of orbits = 1

Time of Simulation = period*number of orbits

Intitial Conditions for Euler Angles and Angular Velocity

The initial conditions for Euler Angles and angular velocity of the CubeSat were carefully chosen to represent realistic scenarios encountered in orbit.

phi0 = 0 rad

theta0 = 0 rad

psi0 = 0 rad

Angular Velocity:

p0 = 0.8 rad/s

q0 = -0.2 rad/s

r0 = 0.3 rad/s

Reaction wheels Parameters

The reaction wheels used in the simulation were modeled with parameters that closely resemble those of commercially available CubeSat reaction wheels. Each reaction wheel was characterized by its moment of inertia, maximum torque, and maximum angular velocity.

mr = .13

rr = 42/1000

hr = 19/1000

rpm = 8000 rpm

maxSpeed = rpm*2*pi/60

maxTorque = 0.004 N-m

dc voltage = 5.0 (Volts) This is from a random RW

peak power = 3.25 Watts

MagneTorquers

In addition to reaction wheels, magnetorquers were incorporated into the simulation to provide supplemental attitude control through magnetic interaction with the Earth's Magnetic field. The magnetorquers were modeled with parameters that reflect typical performance characteristics of those used in CubeSat applications.

n = 84 Number of turns

A = 0.02 Area in meters^2

maxCurrent = 150 mAmps

3.2 Orbit and Alttitude

The Figure 3.1 provides a detailed view of the CubeSat's altitude behavior, particularly highlighting the effectiveness of the B-dot controller and reaction wheels in achieving orbital stability. Immediately after deployment, the CubeSat maintains a

stable altitude around 600 km, indicating a successful insertion into the initial orbit. During this phase, minor fluctuations are observed as the CubeSat begins to stabilize its orientation and adjust to space environment dynamics.

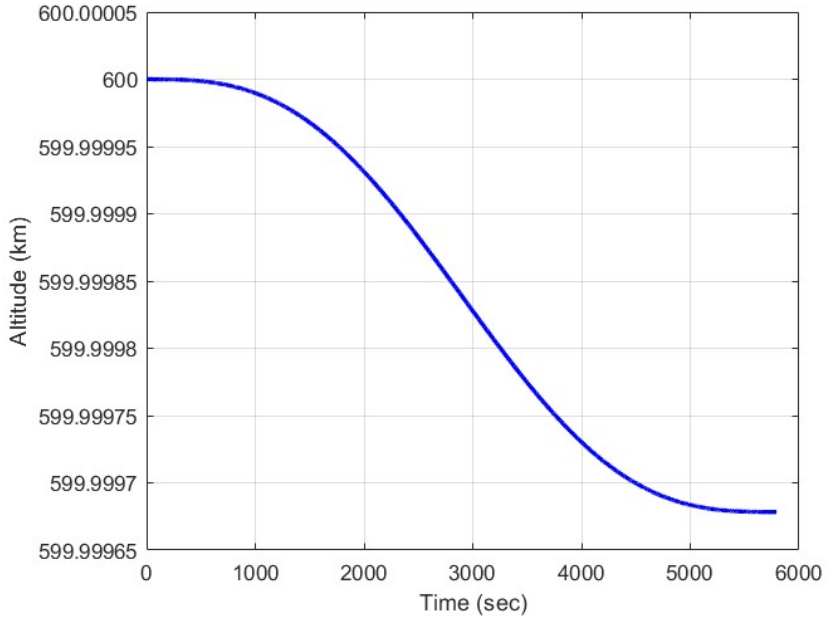

Figure 3.1: CubeSat Alttitude

As time progresses, there is a gradual decrease in altitude from 600 km to approximately 599.99965 km. This descent can be attributed to a combination of factors including residual atmospheric drag, which, even at 600 km, exerts a small but continuous force on the CubeSat, causing a slow orbital decay. The B-dot controller, designed to mitigate rotational disturbances by utilizing Earth's magnetic field, actively works to dampen any residual angular velocity. This magnetic stabilization method helps to align the CubeSat's orientation without relying heavily on its onboard propulsion system, conserving fuel and prolonging the mission duration.

Simultaneously, the reaction wheels, which provide precise control over the CubeSat's attitude, are actively engaged. These wheels spin to create the necessary countertorques that adjust and stabilize the CubeSat's orientation. The coordinated effort of the B-dot controller and reaction wheels ensures that the CubeSat's attitude is corrected efficiently, reducing any wobbling or undesired rotations. This stabilization process is crucial for maintaining proper orientation for communication, power generation from solar panels, and the accurate pointing of scientific instruments or cameras.

Around 5000 seconds into the mission, the CubeSat reaches a new stable altitude,

where the rate of altitude change significantly slows down and eventually plateaus. This indicates that the initial stabilization and adjustment phase is complete, and the CubeSat has settled into a steady orbit at a slightly lower altitude. The reaction wheels have successfully mitigated any remaining rotational disturbances, and the B-dot controller has effectively utilized the Earth's magnetic field to further stabilize the CubeSat's orientation.

The altitude graph of the CubeSat showcases the intricate balance of forces and control mechanisms at play. The B-dot controller and reaction wheels work synergistically to manage the CubeSat's orientation and altitude, ensuring it remains in a stable orbit. The initial descent and subsequent stabilization highlight the efficiency of these control systems in counteracting minor perturbations and achieving a stable operational state. This stability is vital for the CubeSat's mission, enabling it to perform its scientific, observational, or communication tasks effectively throughout its time in orbit.

The provided Figure 3.2 illustrates a three-dimensional plot of a satellite's or-

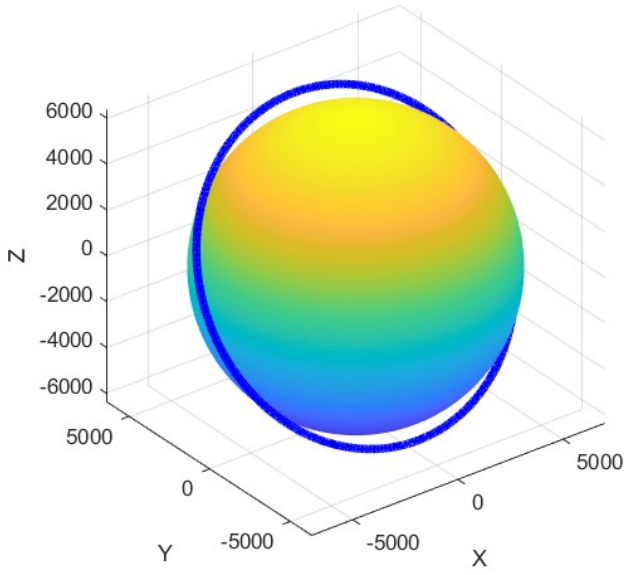

Figure 3.2: CubeSat Orbit

bit around a central body, likely Earth. The orbit is represented by a blue line that traces a nearly perfect circular path, indicating a consistent altitude and distance from the central body throughout the orbit. The central body itself is depicted as a yellow sphere, which serves as the focal point of the satellite's motion. The plot's axes, labeled

X, Y, and Z, represent the three spatial dimensions, allowing a comprehensive view of the orbit's orientation and shape in space. The circular nature of the orbit suggests that the satellite is in a stable, low-inclination orbit, likely equatorial, as there is no noticeable tilt away from the central body's equatorial plane. This visualization is essential for understanding the satellite's motion dynamics and planning any necessary orbital adjustments or maneuvers.

3.3 Magnetic Field using IGRF Model

The International Geomagnetic Reference Field (IGRF) model in MATLAB is a mathematical model used to represent the Earth's main magnetic field. This model is widely used in geophysics, space sciences, and engineering applications to predict the geomagnetic field at any point on or near the Earth's surface.

The IGRF is a series of mathematical models that represent the Earth's magnetic field over time. It is regularly updated by a consortium of international geomagnetic institutes, typically every five years, to account for changes in the Earth's magnetic field. The model is based on spherical harmonics and provides coefficients that describe the geomagnetic field's strength and direction.

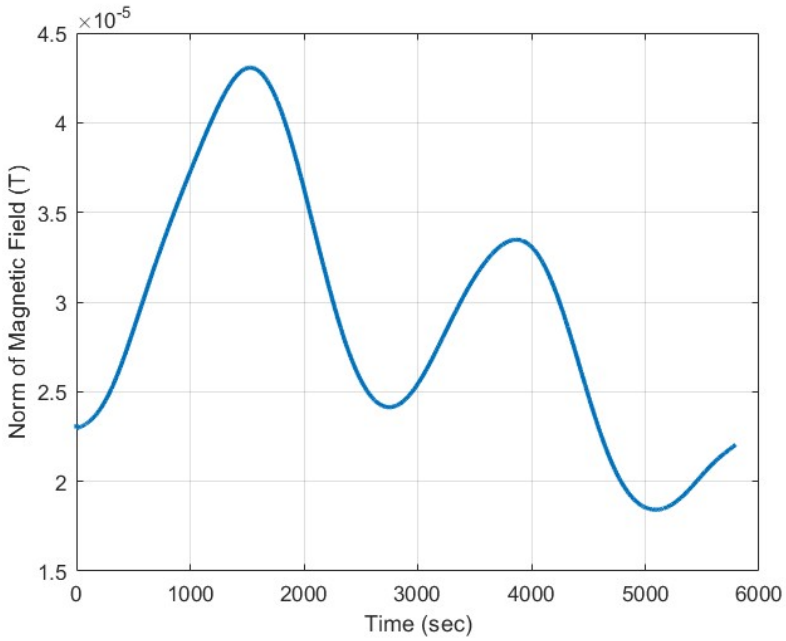

Figure 3.3: Norm of Magnetic Field

The figure 3.3 illustrates the norm of the magnetic field experienced by the CubeSat

over a period of 6000 seconds. The magnetic field norm, measured in teslas (T), exhibits periodic fluctuations, indicative of the CubeSat's interactions with the Earth's geomagnetic field. Initially, the magnetic field strength increases, reaching a peak around 2000 seconds, followed by a decrease to a local minimum at approximately 3000 seconds. This pattern repeats, showing another peak near 4000 seconds before descending again.

These fluctuations are characteristic of the CubeSat's orbital path, as it traverses different regions of the Earth's magnetic field. The variations can be attributed to the CubeSat's movement through areas of varying magnetic field intensity, influenced by its altitude, latitude, and the orientation of its orbit relative to the Earth's magnetic field lines.

Additionally, the B-dot controller and reaction wheels onboard the CubeSat are likely responding to these changes. The B-dot controller, which uses changes in the magnetic field to stabilize the CubeSat, and the reaction wheels, which adjust the satellite's orientation, both depend on accurate measurements of the magnetic field. The periodic changes in the magnetic field norm suggest that the CubeSat is effectively utilizing these control mechanisms to maintain its intended orientation and stability, as it continuously encounters different magnetic field strengths throughout its orbit.

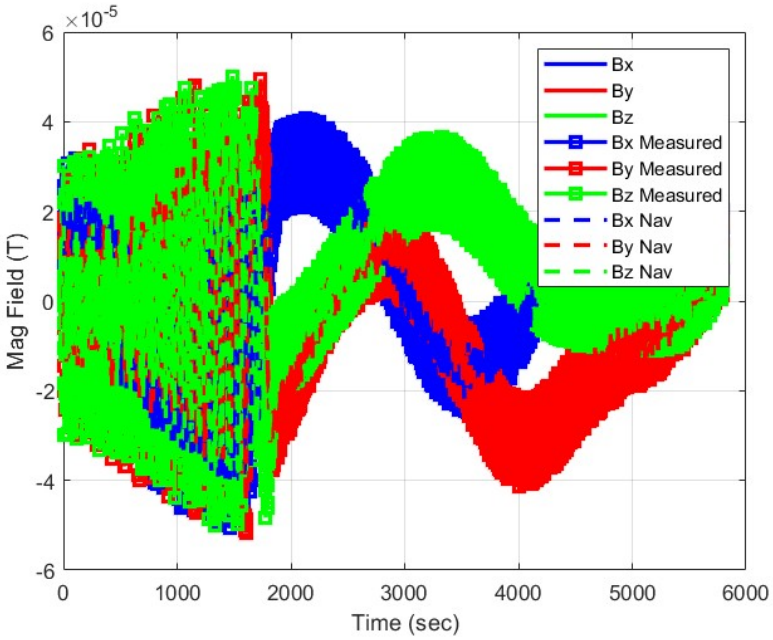

Figure 3.4: Magnetic Field

The Figure 3.4 illustrates the magnetic field components (Bx, By, Bz) of a Cube-

Sat in orbit, where its attitude is controlled using reaction wheels and a B-dot controller. The X-axis represents time in seconds, while the Y-axis shows the magnetic field strength in Tesla.

The solid lines in blue, red, and green indicate the predicted magnetic field components, while the square markers of the same colors represent the measured values. Additionally, the dashed lines depict the navigated or estimated values of these components.

Initially, during the first 1000 seconds, the magnetic field measurements exhibit significant fluctuations and noise. This phase likely corresponds to the initial deployment or activation of the control systems, where the CubeSat is working to stabilize its orientation. As time progresses into the 1000 to 3000-second range, the magnetic field values begin to stabilize, showing more coherent and less noisy patterns. This indicates that the control mechanisms, including the reaction wheels and B-dot controller, are effectively reducing the satellite's angular velocity and aligning it to the desired orientation.

In the final phase, from 3000 to 6000 seconds, the magnetic field components exhibit smoother oscillations, signifying that the CubeSat has achieved a stable and controlled orientation. The measured magnetic field values (represented by square markers) closely follow the predicted and navigated values (solid and dashed lines), demonstrating the efficacy of the control systems.

The reaction wheels provide precise control by altering the CubeSat's angular momentum, while the B-dot controller dampens rotational rates by interacting with the Earth's magnetic field, generating a magnetic moment opposite to the rate of change of the magnetic field. This combined control approach effectively brings the CubeSat to a stable state, as evidenced by the diminishing noise and fluctuations in the magnetic field measurements over time. The graph overall indicates successful attitude control, with the CubeSat's orientation being maintained as intended.

3.4 Euler Angles and Angular Velocity of CubeSat

3.4.1 Euler Angles

This Figure 3.5 illustrates the Euler angles (roll, pitch, and yaw) of a CubeSat over time, where its attitude is controlled using reaction wheels and a B-dot controller. The X-axis represents time in seconds, while the Y-axis shows the Euler angles in degrees, ranging from -200 to 200 degrees. The graph displays three sets of data: the actual Euler angles (solid cyan lines), the measured Euler angles (square purple markers), and the navigated or estimated Euler angles (dashed red lines).

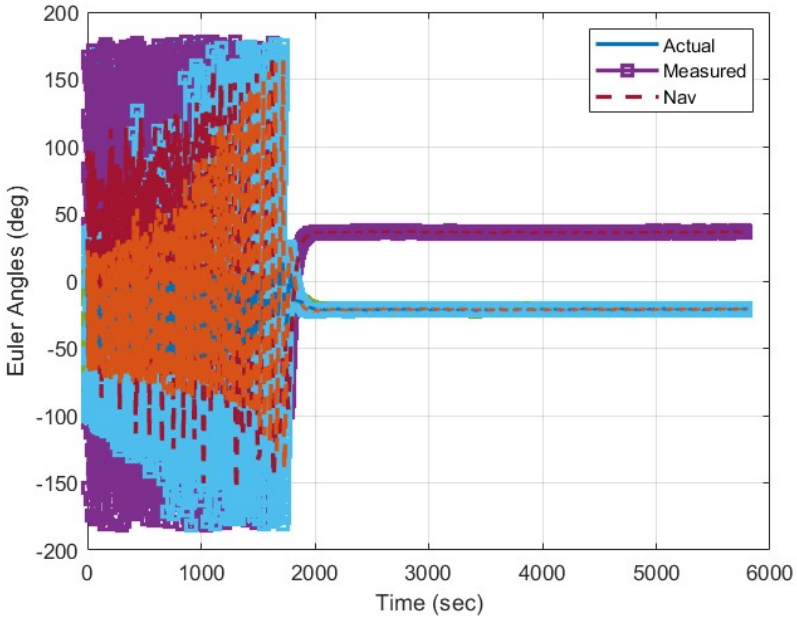

Figure 3.5: Euler Angles of CubeSat

During the initial phase, the Euler angles exhibit significant fluctuations and noise, reflecting the CubeSat's initial instability and the process of its attitude control systems coming online. The actual, measured, and navigated angles are all highly variable, indicating that the CubeSat is undergoing significant rotational motion, likely due to the initial deployment or the activation of its control mechanisms.

Between 1000 and 2000 seconds, the data shows a transition phase where the Euler angles begin to converge. The previously chaotic measurements start to align more closely with the actual and navigated values, suggesting that the control systems are effectively reducing the CubeSat's rotational velocities and stabilizing its orientation. The fluctuations decrease significantly, and the Euler angles settle towards their target

values.

In the final phase, from 2000 to 6000 seconds, the Euler angles stabilize further and maintain steady values. The actual Euler angles (cyan lines) are closely followed by the measured (purple markers) and navigated (red dashed lines) values, indicating successful attitude control. The CubeSat maintains a stable orientation, with the control systems (reaction wheels and B-dot controller) effectively keeping the Euler angles within desired limits. The minimal deviation between the actual, measured, and navigated angles demonstrates the accuracy and efficiency of the control mechanisms.

3.4.2 Angular Velocity

This Figure 3.6 displays the angular velocity of a CubeSat over time, with its attitude controlled by reaction wheels and a B-dot controller. The X-axis represents time in seconds, while the Y-axis shows the angular velocity in radians per second (rad/s). The graph includes three sets of data: actual angular velocity (solid cyan line), measured angular velocity (square purple markers), and navigated or estimated angular velocity (dashed red line).

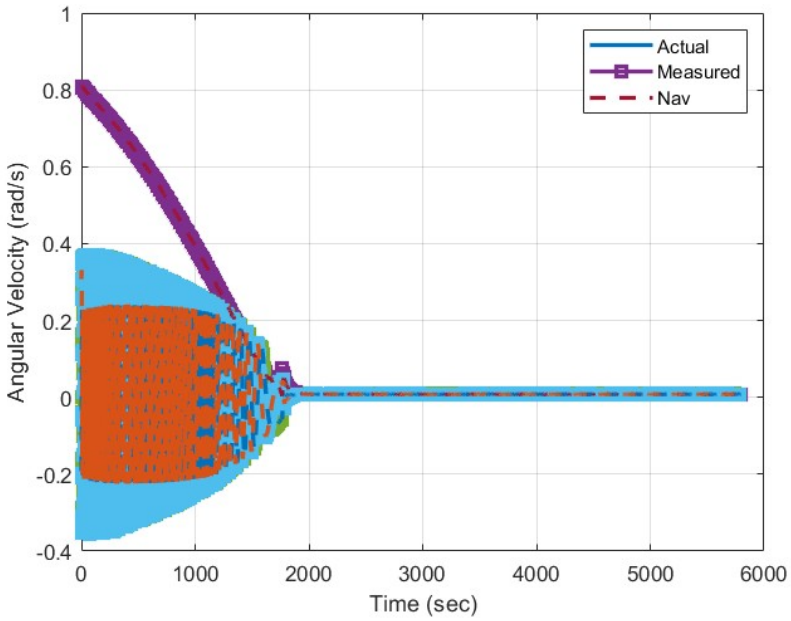

Figure 3.6: Angluar Velocity of CubeSat

In the initial phase, the CubeSat experiences significant fluctuations in angular velocity. The actual, measured, and navigated angular velocities exhibit high variability,

indicating that the CubeSat is undergoing substantial rotational motion. This period likely corresponds to the initial deployment or activation of the control systems, where the CubeSat is still stabilizing and the control mechanisms are working to bring the rotational motion under control.

Between 1000 and 2000 seconds, the graph shows a clear convergence of angular velocities. The fluctuations reduce significantly, and the measured (purple markers) and navigated (red dashed lines) values begin to align closely with the actual (cyan line) values. This indicates that the reaction wheels and B-dot controller are effectively reducing the CubeSat's angular velocity, stabilizing its rotation and bringing it closer to a desired steady state.

From 2000 to 6000 seconds, the CubeSat's angular velocity stabilizes further and maintains a near-zero value, indicating a steady and controlled state. The measured and navigated angular velocities closely follow the actual angular velocity, demonstrating that the control systems are successfully maintaining the CubeSat's orientation with minimal rotational motion. The close alignment between the actual, measured, and navigated values suggests that the CubeSat's attitude control mechanisms are performing efficiently and accurately.

3.5 B-Dot Stabilizing Controller

The Figure 3.7 depicts the current in milliAmperes (mA) applied to the magnetorquers along the X, Y, and Z axes of a CubeSat over a period of 6000 seconds. Initially, up to around 2000 seconds, the current in all three axes fluctuates significantly.The CubeSat is undergoing active attitude control to stabilize its orientation. This period of high activity is likely due to initial disturbances or misalignments that the control system is correcting.

After approximately 2000 seconds, the currents stabilize and oscillate around zero, indicating that the CubeSat has reached a more stable state with minor adjustments being made to maintain its attitude. The gradual decrease in the amplitude of oscillations in the currents indicates that the control system is effectively damping out any residual rotational motion. The currents for the X (blue line), Y (red line), and Z (yellow line) axes show distinct patterns, reflecting the different torques required along

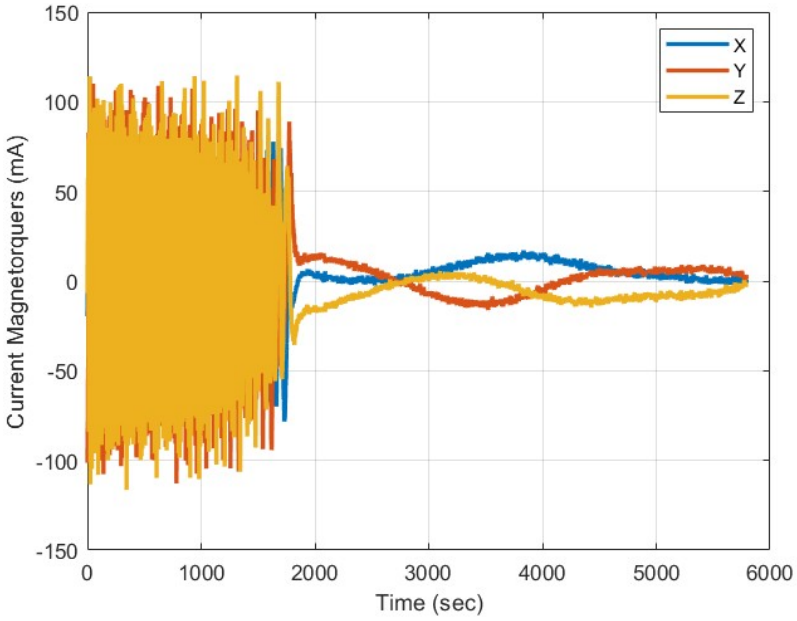

Figure 3.7: The current of Magnetorquers

each axis to maintain stability. Overall, this graph illustrates the dynamic response and eventual stabilization of a CubeSat's attitude using magnetorquers, highlighting the effectiveness of the control system in bringing the satellite to a steady state.

The Figure 3.8 illustrates the total current consumed by the magnetorquers of a CubeSat over a span of 6000 seconds. Initially, the current is high, approximately around 120 mA, indicating significant power consumption by the magnetorquers. This phase lasts up to around 2000 seconds, during which the system is likely engaging in intensive attitude control maneuvers to counteract initial disturbances or to stabilize the CubeSat from an unstable state.

Between 2000 and 3000 seconds, there is a marked decrease in the total current, dropping down to nearly 10 mA. This reduction suggests that the CubeSat has reached a more stable attitude, requiring less power for minor adjustments. The subsequent increase and fluctuations in current between 3000 and 5000 seconds indicate that the CubeSat is experiencing additional disturbances or is making periodic corrections to maintain its orientation. However, the power consumption during this phase is significantly lower compared to the initial phase.

After 5000 seconds, the current gradually decreases, stabilizing around a lower value. This final phase reflects the CubeSat's transition into a stable state with minimal power usage, indicating effective control and maintenance of its attitude.

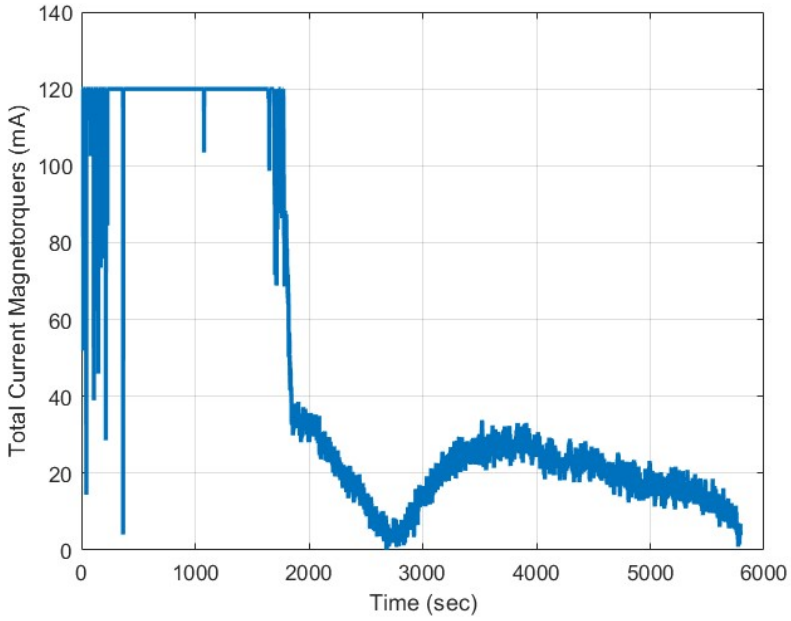

Figure 3.8: Total current of Magnetorquers

3.6 Reaction Wheels

3.6.1 Angular Accelertion and Velocity of Reaction Wheels

The Figure 3.9 shows the angular acceleration of the CubeSat's reaction wheels along the X, Y, and Z axes, measured in radians per second squared (rad/s^2) over a duration of 6000 seconds. Initially, from 0 to approximately 2000 seconds, the angular acceleration for all three axes remains relatively close to zero, indicating minimal adjustments by the reaction wheels during this period. This stability is consistent with the earlier graph showing high current usage by the magnetorquers, suggesting that the magnetorquers are primarily responsible for attitude control during this phase.

Around the 2000-second mark, there is a significant spike in angular acceleration, especially in the Y (red line) and Z (yellow line) axes. This sharp increase implies a sudden and intense correction made by the reaction wheels, possibly in response to a large disturbance or as part of a planned maneuver. The spike reaches values above 6 rad/s^2 for the Y-axis and below -5 rad/s^2 for the Z-axis, while the X-axis (blue line) shows a relatively smaller peak.

Following this intense correction, the angular acceleration rapidly returns to near-zero levels and remains stable for the remainder of the observation period, from 2000 to 6000 seconds. This long-term stability indicates that the CubeSat has achieved

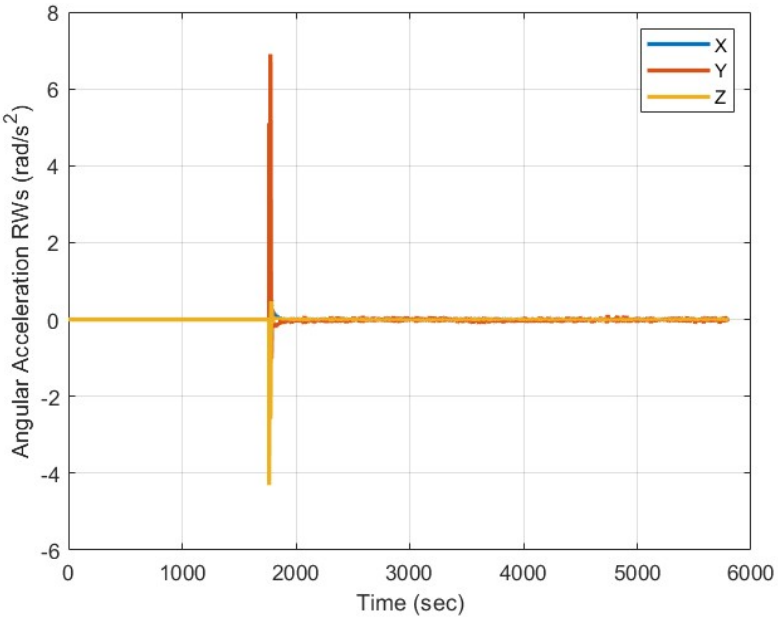

Figure 3.9: Angluar Acceleration of Reaction Wheels

a steady-state condition where only minor adjustments are necessary to maintain its orientation. The brief yet intense activity around the 2000-second mark suggests that the reaction wheels effectively handled a significant attitude control event, after which they settled into a maintenance mode with minimal acceleration required.

The Figure 3.10 depicts the angular velocity of reaction wheels (RWs) in a CubeSat over a period of 6000 seconds. The angular velocity is measured in radians per second (rad/s) and is plotted for three axes: X (blue), Y (red), and Z (yellow).

Initially, all three axes show minimal angular velocity, indicating that the CubeSat is in a relatively stable state with little to no rotation. Around the 2000-second mark, there is a significant spike in the Y-axis angular velocity, reaching approximately 27 rad/s. This sudden increase suggests a substantial control input or disturbance requiring a rapid adjustment. The reaction wheel on the Y-axis works to counteract this disturbance, causing the angular velocity to rise sharply before gradually decreasing.

Following this peak, the Y-axis angular velocity starts to decline and eventually stabilizes around zero after oscillating and dampening out. The X-axis angular velocity exhibits a smaller increase, stabilizing at a slightly negative value, around -5 rad/s. This implies a minor correction in the X-axis rotation. The Z-axis shows a similar trend to the X-axis, with a smaller magnitude of change and eventual stabilization around -2 rad/s.

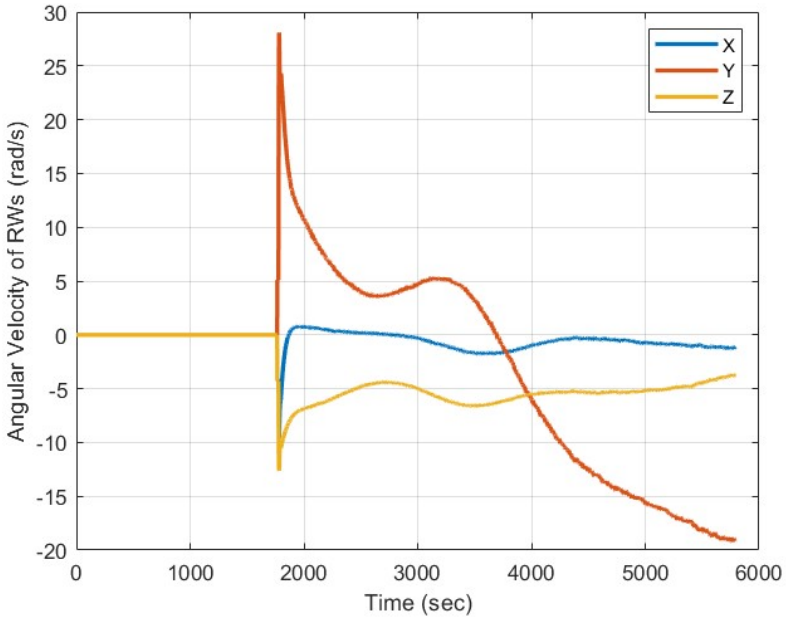

Figure 3.10: Angluar Velocity Of Reaction Wheels

The damping oscillations observed in all three axes indicate the system's effort to achieve stabilization after the initial disturbance. Over time, the angular velocities on all axes converge towards steady-state values, indicating successful stabilization and control by the reaction wheels. The differences in the magnitudes and stabilization times across the axes reflect the specific dynamics and control strategies implemented in the CubeSat's attitude control system.

3.6.2 Current of Reaction Wheels

The Figure 3.11 illustrates the current consumption of the reaction wheels (RWs) in a CubeSat over a period of 6000 seconds, with the current measured in milliamps (mA) for three axes: X (blue), Y (red), and Z (yellow).

Initially, the current for all three axes is close to zero, indicating that the reaction wheels are either idle or maintaining a very low level of activity to keep the CubeSat stable. Around the 2000-second mark, a significant event occurs that causes a sharp increase in the current, particularly in the Y-axis, which peaks at approximately 125 mA. This spike suggests that the reaction wheel on the Y-axis is exerting a substantial torque to counteract a disturbance or to execute a rapid maneuver, demanding a higher current draw to achieve the necessary rotational speed.

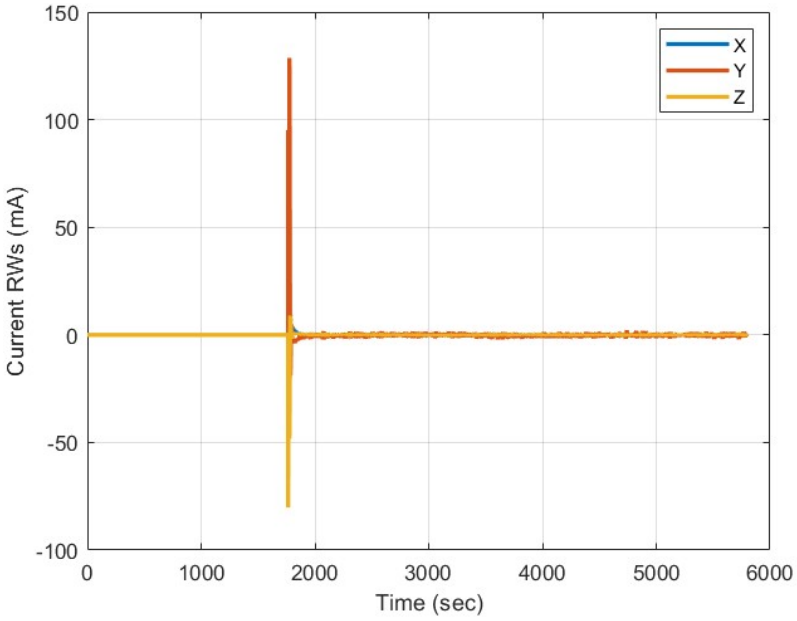

Figure 3.11: Current of Reaction Wheels

The Z-axis also shows a notable, albeit smaller, negative spike in current, reaching around -50 mA, indicating that the reaction wheel on this axis is also actively involved in counteracting the disturbance but in the opposite direction. The X-axis experiences a smaller positive increase in current, peaking around 20 mA, suggesting a less significant but still active role in the stabilization process.

After this disturbance, the current on all axes returns to near zero, reflecting the reaction wheels settling back to a low power state as the CubeSat stabilizes. The current levels post-disturbance show minor fluctuations, indicating continuous, minor adjustments to maintain stability.

The significant spikes and subsequent return to baseline illustrate the dynamic response of the reaction wheel system to disturbances. The higher current in the Y-axis compared to the X and Z axes indicates that the Y-axis reaction wheel bore the brunt of the stabilization effort, likely due to the nature of the disturbance or the control strategy employed. The ability of the reaction wheels to quickly ramp up current and then return to a low-power state demonstrates the effectiveness and efficiency of the CubeSat's attitude control system.

The Figure 3.11 displays the total current consumption of the reaction wheels (RWs) in a CubeSat over a period of 6000 seconds, measured in milliamps (mA). The total current is the sum of the currents drawn by the individual reaction wheels along the

X, Y, and Z axes.

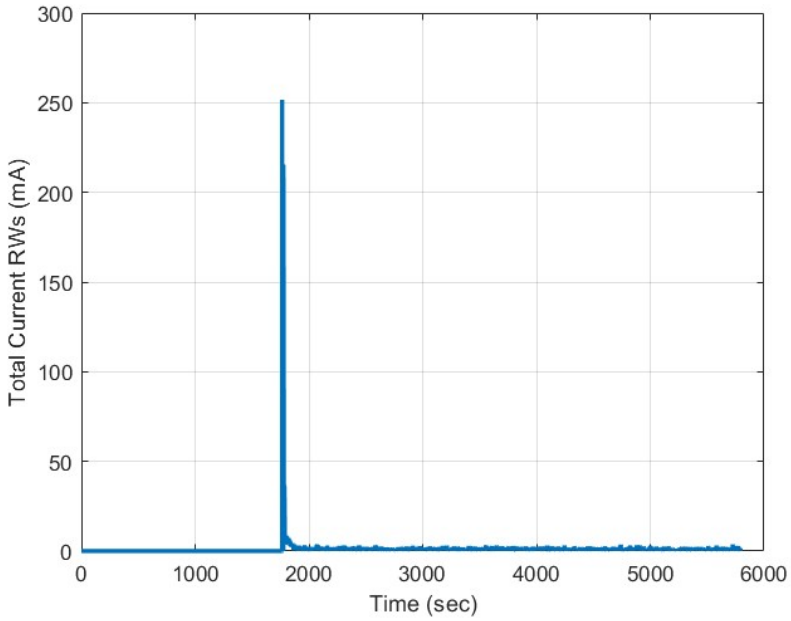

Figure 3.12: Total Current of Reaction Wheels

For the initial 2000 seconds, the total current remains close to zero, indicating that the reaction wheels are operating at minimal levels, likely maintaining the CubeSat's attitude without significant disturbances. Around the 2000-second mark, there is a dramatic spike in the total current, reaching a peak of approximately 250 mA. This surge signifies a substantial demand for power as the reaction wheels respond to a major disturbance or execute a rapid maneuver.

The sharp increase in current aligns with the earlier observations of individual axis currents, where the Y-axis exhibited a significant increase, suggesting that the primary control effort was required along this axis. The total current quickly rises to its peak and then just as rapidly begins to decline, indicating that the reaction wheels are quickly working to counteract the disturbance and stabilize the CubeSat.

Following the peak, the total current sharply drops and stabilizes back to a low level, around 10-20 mA, for the remainder of the time period. This low, steady current indicates that the CubeSat has returned to a stable state, with the reaction wheels maintaining attitude control with minimal effort.

The single, prominent peak in the graph highlights the CubeSat's ability to handle significant disturbances efficiently. The rapid return to low current consumption demonstrates the effectiveness of the reaction wheel system in stabilizing the CubeSat

quickly, thus minimizing power usage after the initial response. This efficient handling of disturbances is critical for the CubeSat's overall power management and longevity in space.

The Figure 3.13 shows the total current consumption of both magnetorquers and reaction wheels on a CubeSat over a period of 6000 seconds. Initially, the current fluctuates significantly, with values mostly below 100 mA, indicating active adjustments in the early phase, likely during the initial stabilization period of the CubeSat. Around the 1000-second mark, the current stabilizes at approximately 100 mA, suggesting that the CubeSat has achieved a steady state in its attitude control, with both the magnetorquers and reaction wheels working in a balanced manner.

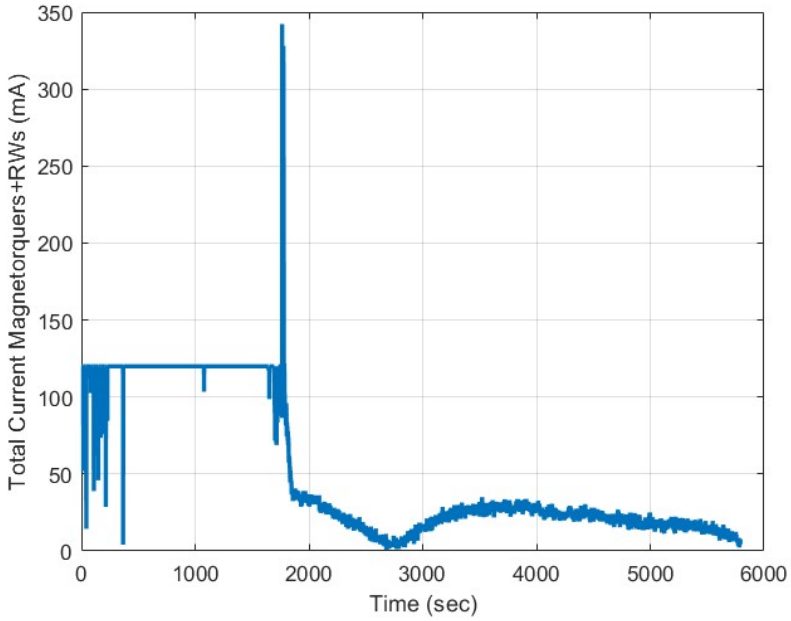

Figure 3.13: Total Current of Magnetorquers and Reaction Wheels

A notable spike in current is observed around 1800 seconds, where it peaks to around 350 mA. This sudden increase suggests a significant event or a major adjustment in the attitude control system, possibly due to an external disturbance or a commanded change in the CubeSat's orientation. After this peak, the current rapidly decreases, eventually dropping to nearly zero around the 2500-second mark. This sharp decline implies that the system might have entered a different operational mode or the attitude control demand significantly reduced.

Following this event, the current stabilizes again but at a much lower level, around 50 mA. This reduced level persists for the remainder of the observation period, indi-

cating a low power consumption phase for the attitude control system. The smoother curve in this phase suggests less frequent adjustments, implying that the CubeSat's attitude has become more stable or that the reaction wheels and magnetorquers are operating more efficiently.

3.7 Hardware Description

The hardware setup for the Attitude Determination and Control (ADC) system of the CubeSat consists of several key components designed to ensure precise orientation and stability in space. The primary actuators are three reaction wheels, each mounted orthogonally to provide independent control over the satellite's pitch, yaw, and roll axes. These reaction wheels are capable of generating precise torques, allowing for fine adjustments to the CubeSat's attitude. Complementing the reaction wheels, magnetorquers are integrated into the system to assist with detumbling and to provide additional control by interacting with the Earth's magnetic field. For attitude determination, the CubeSat is equipped with gyroscopes to measure angular velocity and star trackers to provide accurate orientation data by observing the positions of stars. These sensors feed data into an onboard computer, which runs advanced control algorithms, including a Proportional-Integral-Derivative (PID) controller

3.7.1 2U CubeSat Structure

The design of a 2U CubeSat is crucial for its functionality, ensuring structural integrity, compatibility with launch systems, and protection of internal components in space. This comprehensive explanation explores the intricate construction and characteristics of the CubeSat structure.The skeleton of a 2U CubeSat is its frame, typically made of aerospace-grade aluminum alloys for strength and lightness. Comprising longitudinal beams, lateral struts, and corner brackets, the frame is meticulously engineered to endure the stresses of launch and operation. The frame is built in a modular manner, with each 1U section featuring precisely machined components connected with high-strength fasteners like screws, bolts, and rivets. This modular approach simplifies manufacturing and assembly, while also allowing easy access for maintenance and upgrades. For our project, we have selected the ZAPHOD 2U CubeSat Structure designed

by AAC Clyde Space.

Zaphod 2U CubeSat Structure

The ZAPHOD 2U CubeSat Structure is fully compatible with all rail-deployers, ensuring seamless deployment. The inclusion of deployment switches guarantees compatibility with manned flights and the International Space Station (ISS). This structure has been meticulously designed with a high level of modularity, allowing for the accommodation of even the most unique payload configurations. Its lightweight and qualified design maximizes internal volume, providing ample space for various components. Additionally, the ease of access during integration and customizable internal stack layout further enhance its versatility.

Technical Specifications

- Aluminum 7075 and 6082 used for primary structures
- All other materials comply with typical out-gassing requirements
- Designed and qualified to NASA GEVS, 14.1gRMS
- Temperature range -40C to +80C
- Four deployment switches, two on the -Z end plate and two on the rails

Length	100 mm
Width	100 mm
Height	227 mm
Weight	235 g

Table 3.1: Size and Weight of the Zaphod 2U CubeSat Structure

3.7.2 Arduino uno rev3

The Arduino UNO rev3 is an ideal board for gaining familiarity with electronics and coding. This versatile development board features the well-known ATmega328P and the ATMega 16U2 Processor. The Arduino Uno is a microcontroller board that is based on the ATmega328P microchip. It offers 14 digital input/output pins (with 6

Figure 3.14: the Zaphod 2u cubesat structure

of them capable of being used as PWM outputs), 6 analog inputs, a 16 MHz quartz crystal, a USB connection, a power jack, an ICSP header, and a reset button. It includes everything necessary to support the microcontroller. To get started, all we need to do is connect it to a computer using a USB cable or power it with an AC-to-DC adapter or battery. With the UNO, we can experiment without worrying too much about making mistakes. In the worst-case scenario, we can easily replace the chip for a small cost and start over again. The term "Uno" means "one" in Italian and was chosen to commemorate the release of Arduino Software (IDE) 1.0. The Uno board, along with version 1.0 of Arduino Software (IDE), served as the reference versions of Arduino and have since evolved into newer releases. The Uno board is the first in a series of USB Arduino boards and serves as the standard model for the Arduino platform. For a comprehensive list of current, past, or outdated boards, please refer to the Arduino index of boards.

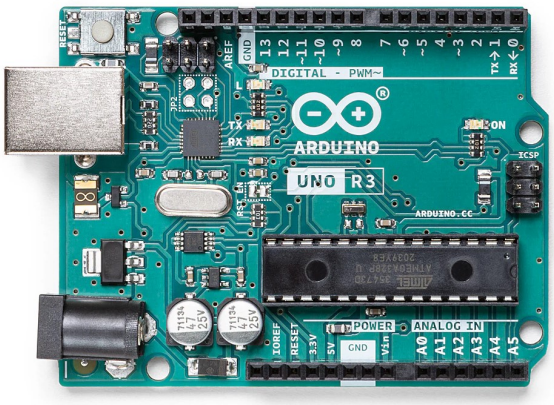

Figure 3.15: Arduino uno rev3 front view

Connector Pinouts

Pin	Function	Type	Description
1	NC	NC	Not connected
2	IOREF	IOREF	Reference for digital logic V - connected to 5V
3	Reset	Reset	Reset
4	+3V3	Power	+3V3 Power Rail
5	+5V	Power	+5V Power Rail
6	GND	Power	Ground
7	GND	Power	Ground
8	VIN	Power	Voltage Input
9	A0	Analog/GPIO	Analog input 0 / GPIO
10	A1	Analog/GPIO	Analog input 1 / GPIO
11	A2	Analog/GPIO	Analog input 2 / GPIO
12	A3	Analog/GPIO	Analog input 3 / GPIO
13	A4/SDA	Analog input/I2C	Analog input 4 / I2C Data line
14	A5/SCL	Analog input/I2C	Analog input 5 / I2C Clock line

Table 3.2: JANALOG

Pin	Function	Type	Description
1	D0	Digital/GPIO	Digital pin 0/GPIO
2	D1	Digital/GPIO	Digital pin 1/GPIO
3	D2	Digital/GPIO	Digital pin 2/GPIO
4	D3	Digital/GPIO	Digital pin 3/GPIO
5	D4	Digital/GPIO	Digital pin 4/GPIO
6	D5	Digital/GPIO	Digital pin 5/GPIO
7	D6	Digital/GPIO	Digital pin 6/GPIO
8	D7	Digital/GPIO	Digital pin 7/GPIO
9	D8	Digital/GPIO	Digital pin 8/GPIO
10	D9	Digital/GPIO	Digital pin 9/GPIO
11	SS	Digital	SPI Chip Select
12	MOSI	Digital	SPI Main Out Secondary In
13	MISO	Digital	SPI Main In Secondary Out
14	SCK	Digital	SPI serial clock output
15	GND	Power	Ground
16	AREF	Digital	Analog reference voltage
17	A4/SD4	Digital	Analog input 4/I2C Data line (duplicated)
18	A5/SD5	Digital	Analog input 5/I2C Clock line (duplicated)

Table 3.3: JDIGITAL

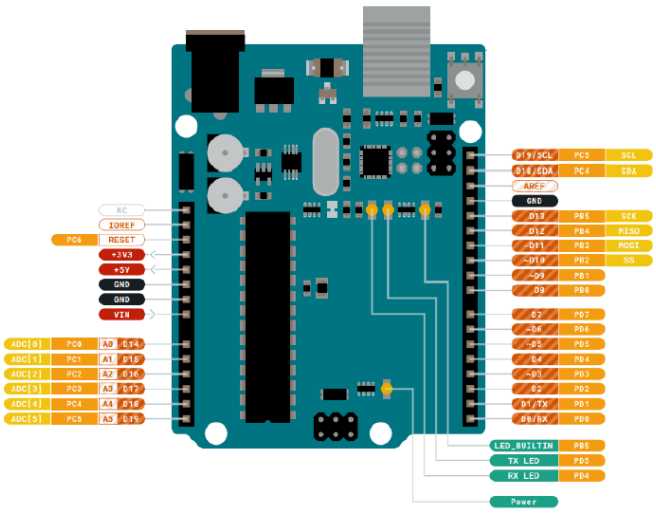

Figure 3.16: arduino uno rev3 pinouts

ARDUINO uno rev3 datasheet

Microcontroller	ATmega328P
Operating Voltage	5V
Input Voltage (recommended)	7-12V
Input Voltage (limit)	6-20V
Digital I/O Pins	14 (of which 6 provide PWM output)
PWM Digital I/O Pins	6
Analog Input Pins	6
DC Current per I/O Pin	20 mA
DC Current for 3.3V Pin	50 mA
Flash Memory	32 KB (ATmega328P) of which 0.5 KB used by bootloader
SRAM	2 KB (ATmega328P)
EEPROM	1 KB (ATmega328P)
Clock Speed	16 MHz
LED BUILTIN	13
Width	53.4 mm
Weight	25 g
Weight	235 g

Table 3.4: ARDUINO Uno Rev3 datasheet

3.7.3 Magnetorquer(CubeTorquer gen1)

CubeTorquer is a nanosatellite magnetic torquer made by cubespace that uses a specially treated ferrous core with ultra-low remanence and high linearity. It can be used for detumbling, coarse attitude changes and to desaturate reaction wheels, we chose the cubetorquer gen1 for:

- its ULTRA-LOW REMANENCE

  When it comes to magnetic control on satellites, it is most important to remove all unwanted magnetic disturbances. One of the most common disturbances is remanent magnetic dipoles left in parts of the satellite after a torquer has been pulsed. We use a highly specialized material for the ferrous core of our rods,

which we treat to give our rods ultra-low remanence.

- its compactness

  In small satellites, compactness is a strong requirement. The way the standard CubeSat boards are stacked makes it difficult to have three rods to form a 3-Axis system. We offer a low-profile air-core coil that slots into the stack between the CubeSat PCBs. In this way, we can create a very compact 3-Axis magnetic control system.

we selected the cubetorquer gen1 size s for our project.

Figure 3.17: CubeTorquer gen1

3.7.4 Cubetorquer Gen1 Datasheet

Minimum Magnetic Moment [Am2] @ 5V	±0.24
Magnetic Gain [Am^2/A]	2.8
Nominal Resistance [ohm]	29-31
Mass [g]	28
Analog Input Pins	6
Dimensions [WxLxH] [mm]	18x14x62
Max Current [mA]	150
Radiation	24kRad
Random Vibration	14g RMS
Price	USD 870

Table 3.5: Cubetorquer Gen1 Size S Datasheet

3.7.5 Ultra-low Disturbance Reaction Wheel (RWp015)

Made by blue kanyon , This ultra low disturbance reaction wheel feature an advanced lubrication system for long life and vibration isolation. It has supported missions ranging from very low Earth orbit to cislunar and interplanetary journeys , it was made with Brushless DC motors, ultra-smooth bearings and an advanced lubrication system that ensures low jitter performance and long life for any mission .Made in the U.S. and applicable for DOD applications. This reaction wheel is operating on-orbit, supporting numerous successful missions. To date, there is more than 500 Blue Canyon Technologies Reaction Wheels on orbit . and its key advantages are :

- High-accuracy observer-based control design
- Low jitter with fine balance available
- Wheel Life Test ongoing
- High torque-to-speed ratio

Figure 3.18: RWp015

RWp015 Datasheet

MAX MOMENTUM	0.015 Nms
MAX TORQUE	0.004 Nm
CONTROL ACCURACY AT MAX TORQUE	2.0 rad
MASS	0.13 kg
Dimensions	42 x 42 x 19 mm
SUPPLY VOLTAGE	10 - 14 VDC
POWER AT MAX MOMENTUM	$<$ 1 W
PEAK POWER	5.5 W
POWER AT ZERO MOMENTUM	0 W
PEAK REGENERATED POWER	0.88 W
CONNECTOR TYPE	Nano receptacle A29400-031
PROTOCOL	RS-422
ELECTRONICS	DCE
VIBRATION QUALIFICATION	GEVS Qualification Profile
OPERATING TEMPERATURE	-20 °C to +60 °C
SURVIVAL TEMPERATURE	-30 °C to +70 °C
SYSTEM RADIATION HARDNESS (Si)	$>$ 40 Krad
DESIGN LIFE	$>$ 40 Krad

Table 3.6: RWp015 datasheet

3.7.6 Magnetometre (HMC2003)

made by Honeywell , HMC2003 is a high sensitivity, three-axis magnetic sensor hybrid assembly used to measure low magnetic field strengths. Honeywell's most sensitive magneto-resistive sensors (HMC1001 and HMC1002) are utilized to provide the reliability and precision of this magnetometer design. The HMC2003 interface is all analog with critical nodes brought out to the pin interfaces for maximum user flexibility. The internal excitation current source and selected gain and offset resistors, reduces temperature errors plus gain and offset drift. Three precision low-noise instrumentation amplifiers with 1kHz low pass filters provide accurate measurements while rejecting unwanted noise. Applications include: Precision Compassing, Naviga-

tion Systems, Attitude Reference, Traffic Detection, Proximity Detection and Medical Devices. we selected it for its features :

- 20-pin Wide DIP Footprint (1" by 0.75")
- Precision 3-axis Capability
- Factory Calibrated Analog Outputs
- 40 micro-gauss to ±2 gauss Dynamic Range
- Analog Output at 1 Volt/gauss (2.5V @ 0 gauss)
- Onboard +2.5 Volt Reference
- +6 to +15 Volt DC Single Supply Operation
- Very Low Magnetic Material Content
- -40c to 85c Operating Temperature Range

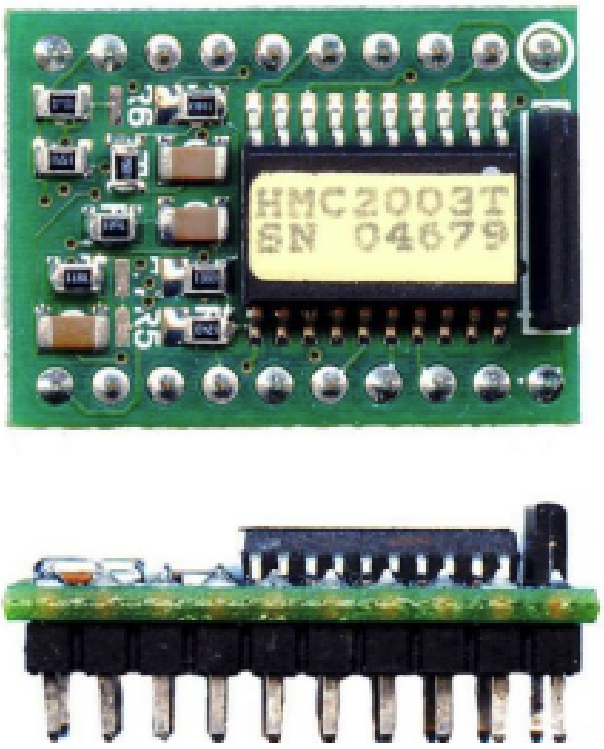

Figure 3.19: HMC2003 Honeywell

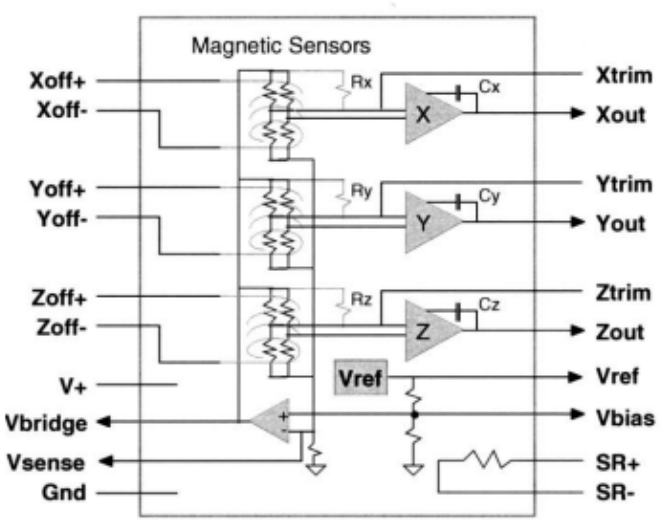

Figure 3.20: HMC2003 Honeywell Block Diagram

HMC2003 Magnetometer Datasheet

Characteristics	Min	Typ	Max
Sensitivity(V/gauss)	0.98	1	1.02
Null Field Output(v)	2.3	2.5	2.7
Resolution(ugauss)	//	40	//
Field Range(gauss)	-2	//	2
Output Voltage(v)	3.92	//	4.08
Bandwidth (kHz)	//	1	//
Resistance(ohms)	//	//	10.5
Sensitivity(mA/gauss)	//	47.5	//
Current(mA)	//	//	200
Resistance(ohms)	//	4.6	6
Current(Amps)	2.0	3.2	4.5
Field Sensitivity(ppm/C)	//	-600	//
Temperature(°C)	-40/-55	//	85/125
Vibration(g rms)	//	2	//
Supply Voltage (VDC)	6	//	15
Supply Current (mA)	//	//	20

Table 3.7: HMC2003 datasheet

3.7.7 Star Tracker (NST)

Made by Blue Canyon Technologies ,Nano Star Tracker (NST) is qualified beyond GEVS level environments, providing a low SWaP-C solution with sunning capabilities. The turnkey starlight-in, quaternion-out system integrates easily and tracks down to 7.5 magnitude. With an on-board star catalog of more than 20,000 stars, this tracker is the ideal fit for standalone missions or constellations. Made in the U.S. and applicable for DOD applications. There are currently more than 150 star trackers on-orbit with more than 250 years of cumulative flight time. The longest mission to date for the NST was launched in 2016 with the Cygnss satellite for hurricane forecasting. it is designed with technical capabilities and radiation tolerance suited to missions in both LEO and GEO. Blue Canyon Technologies Star Trackers include internal control electronics baffles. External baffles on the mid-extension and full-extension units narrow sun and earth exclusion angles. we selected the standard NST for these features :

- Nearly 500 star trackers manufactured with more than 150 on-orbit
- Low SWaP-C
- Tracks stars down to 7.5 magnitude
- On-board star catalog features more than 20,000 stars
- Lost-in-space star idenification
- Shock test qualified
- EMI / EMC tested to MIL-STD-461
- User friendly RS-422 or RS-485 interface

Figure 3.21: standard NST

Standard NST Datasheet

FIELD OF VIEW	10 x 12 deg
SOLUTION RATE	5 Hz
MAX SLEW RATE	$>$ 2 deg/sec
LOST-IN-SPACE STAR IDENTIFICATION	$<$ 4 sec (up to 1.5 deg/sec)
SKY COVERAGE	$>$ 99%
BAFFLE SUN EXCLUSION ANGLE	45 deg
BAFFLE EARTH EXCLUSION ANGLE	25 deg
DIMENSIONS	10 x 5.5 x 5 cm
MASS	0.35 kg
SUPPLY VOLTAGE	5 V or 28 V
PEAK POWER CONSUMPTION	$<$ 1.5 W (5 V) or $<$ 3.5 W (28 V)
SIGNAL INTERFACE	RS-485 or RS-422
OPERATING TEMPERATURE	-20 °C to +50 °C
SURVIVAL TEMPERATURE	-30 °C to +70 °C
VIBRATION QUALIFICATION	GEVS Qualification Profile
DESIGN LIFE	$>$ 10 years (LEO)/$>$ 5 years (GEO)

Table 3.8: Standard NST Datasheet

3.7.8 Gyroscope(MPU6050)

MPU6050 sensor module is complete 6-axis Motion Tracking Device. It combines 3-axis Gyroscope, 3-axis Accelerometer and Digital Motion Processor all in small package. Also, it has additional feature of on-chip Temperature sensor. It has I2C bus interface to communicate with the microcontrollers. It has Auxiliary I2C bus to communicate with other sensor devices like 3-axis Magnetometer, Pressure sensor etc. If 3-axis Magnetometer is connected to auxiliary I2C bus, then MPU6050 can provide complete 9-axis Motion Fusion output.

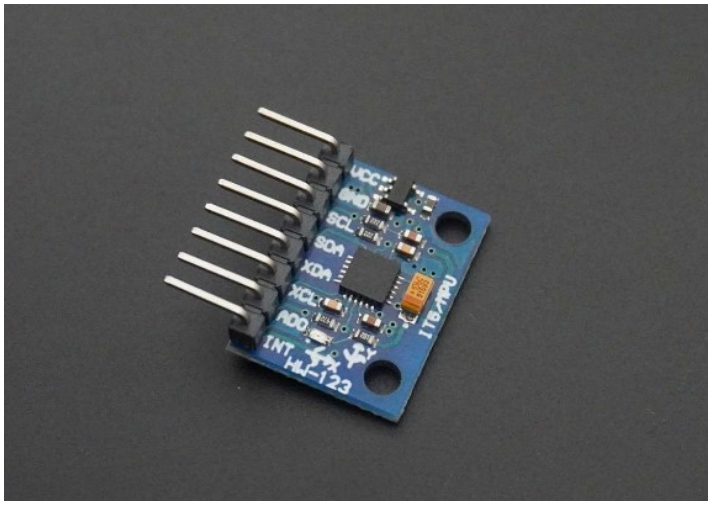

Figure 3.22: MPU6050

MPU6050 Module Pinout

The MPU-6050 module has 8 pins

- INT: Interrupt digital output pin.
- AD0: I2C Slave Address LSB pin. This is 0th bit in 7-bit slave address of device. If connected to VCC then it is read as logic one and slave address changes.
- XCL: Auxiliary Serial Clock pin. This pin is used to connect other I2C interface enabled sensors SCL pin to MPU-6050.
- XDA: Auxiliary Serial Data pin. This pin is used to connect other I2C interface enabled sensors SDA pin to MPU-6050.
- SCL: Serial Clock pin. Connect this pin to microcontrollers SCL pin.

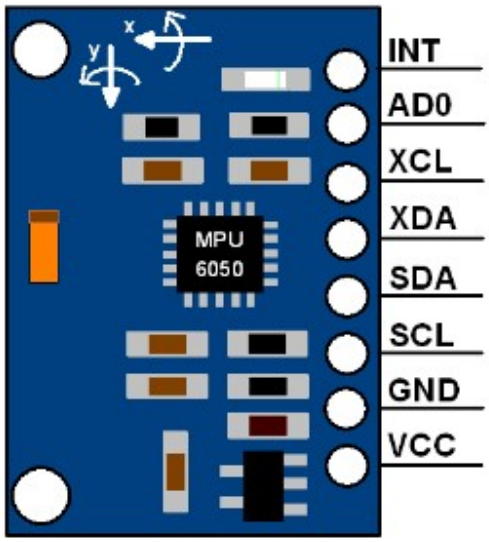

Figure 3.23: MPU6050 Module Pinout

- SDA: Serial Data pin. Connect this pin to microcontrollers SDA pin.
- GND: Ground pin. Connect this pin to ground connection.
- VCC: Power supply pin. Connect this pin to +5V DC supply.
- Slave Write address(SLA+W): 0xD0
- Slave Read address(SLA+R): 0xD1

MPU-6050 has various registers to control and configure its mode of operation

MPU6050 Module features

The triple-axis MEMS gyroscope in the MPU-6050 includes a wide range of features :

- Digital-output X-, Y-, and Z-Axis angular rate sensors (gyroscopes) with a user-programmable fullscale range of ±250, ±500, ±1000, and ±2000°/sec
- External sync signal connected to the FSYNC pin supports image, video and GPS synchronization
- Integrated 16-bit ADCs enable simultaneous sampling of gyros
- Enhanced bias and sensitivity temperature stability reduces the need for user calibration

- Improved low-frequency noise performance
- Digitally-programmable low-pass filter
- Gyroscope operating current: 3.6mA
- Standby current: 5µA
- Factory calibrated sensitivity scale factor
- User self-test
- Sensitivity of 131, 65.5, 32.8, or 16.4 LSBs per dps
- Output data rate (ODR) range of 8kHz to 1.25Hz
- Operating voltage range of 2.375V to 3.46V for the MPU-6050, and 2.375V to 5.5V for the MPU-6050A
- I2C serial interface with a maximum clock frequency of 400kHz
- 8-bit and 16-bit register access modes
- Digital Motion Processor (DMP) for complex motion processing

Conclusion

In this thesis, we successfully Controled the CubeSats using reaction wheels. The primary objective was to enhance the CubeSat's ability to maintain a precise orientation in space, which is crucial for various scientific and commercial applications. The simulations demonstrated the efficacy of our approach. The results showed significant improvements in attitude determination accuracy and control precision. Our system effectively minimized disturbances and corrected deviations, ensuring that the CubeSat maintained its desired orientation with high reliability.

Moreover, the integration of advanced sensor fusion techniques enhanced the accuracy of attitude determination, providing precise real-time data critical for control decisions. The successful implementation of these techniques underscores the potential of reaction wheels as a viable solution for attitude control in small satellites. This research contributes to the broader field of small satellite technology by providing a scalable and efficient method for attitude control. Future work could explore the integration of other control mechanisms, such as thrusters, to further enhance the performance and versatility of CubeSat systems.

Bibliography

[1] M. Swartwout, "The first one hundred CubeSats : A statistical look," J. Small Satell., 2013.

[2] https://www.nanosats.eu

[3] H. J. Kramer and A. P. Cracknell, "An overview of small satellites in remote sensing," International Journal of Remote Sensing. 2008.

[4] CubeSat, "Cubesat design specification," 2014.

[5] "Nanosats Database." https://www.nanosats.eu/.

[6] F. L. Markley and J. L. Crassidis, Fundamentals of spacecraft attitude determination and control. 2014.

[7] L. Federici, B. Benedikter, and A. Zavoli, "Machine Learning Techniques for Autonomous Spacecraft Guidance during Proximity Operations," 2021.

[8] R. Chai, A. Savvaris, A. Tsourdos, S. Chai, and Y. Xia, "A review of optimization techniques in spacecraft flight trajectory design," Progress in Aerospace Sciences. 2019.

[9] Dr.Ing. Toshinori Kuwahara ."Introduction to CubeSat Attitude Control System", KiboCUBE Academy, 2021.

[10] SPACE WEATHER PREDICTION CENTER website. https://www.swpc.noaa.gov

[11] B. Etkins. Dynamics of Atmospheric Flight. Dover, Mineola, New York, 2000.

[12] Warren F. Phillips. Mechanics of Flight. John Wiley and Sons Hoboken New Jersey, 2010.

[13] R.C. Nelson. Flight Stability and Automatic Control. McGraw-Hill, 2nd edition, 1998.

[14] Jerry E. White Roger R. Bate, Donald D. Mueller. Fundamentals of Astrodynamics. Dover, 1971.

[15] Arthur KL Lin and Regina Lee. Attitude control for small spacecraft with sensor errors. In AIAA SPACE Conferences and Exposition, Pasadena, California, August 2015

[16] Nuno Filipe and Panagiotis Tsiotras. Adaptive position and attitude-tracking controller for satellite proximity operations using dual quaternions. Journal of Guidance, Control, and Dynamics.

[17] 0. A. Bachau. Flexible Multibody Dynamics. Springer, 2008.

[18] Karsten Grosekathofer and Zizung Yoon. Introduction into quaternions for spacecraft attitude representation. Technical University of Berlin Department of Astronautice and Aeronautics, 2012.

[19] John L. Cassidis and John L. Junkins. Optimal Estimation of Dynamic Systems. Chapman and Hall/CRC, 2004.

[20] Sebastian Munoz and E. Glenn Lightsey. A sensor driven trade study for autonomous navigation capabilities. AIAA.

[21] John L. Cassidis, F. Landis Markley, and Yang Chen. Survey of nonlinear attitude estimation methods. Journal of Guidance, Control, and Dynamics, 2007.

[22] Bing Liu, Zhen Chen, Xiangdong Liu, and Fan Yang. An efficient nonlinear filter for spacecraft attitude estimation. International Journal of Aerospace Engineering, 2014.

[23] R. M. Georgevic. The solar radiation pressure forces and torques model. The Journal of the Astronautical Sciences, 1973.

[24] Anderson D. Fundamentals of Aerodynamics 4th Edition. McGraw Hill Series, 2007.

[25] Graham Gyatt. The standard atmosphere. A mathematical model of the 1976 U.S. Standard Atmosphere, Jan 2006.

[26] Geographic library c++. Jul 11, 2017

[27] L. G. Jacchia. Static diffusion models of the upper atmosphere with empirical temperature profiles. Smithson. Astrophys. Obs. Spec. Rept. 1964. Cambridge, Massachusetts.

[28] L. G. Jacchia. Revised static models of the thermosphere and exosphere with empirical temperature profiles. Smithson. Astrophys. Obs. Spec. Rept., 1971. Cambridge, Massachusetts.

[29] L. G. Jacchia. Thermospheric temperature, density, and composition: New models. Smithson. Astrophys. Obs. Spec. Rept. 1977. Cambridge, Massachusetts.

[30] Enhanced magnetic field model. https://www.ngdc.noaa.gov/geomag/EMM/ .cited Jul 11, 2017.

[31] Earth gravity model. https://www.ngdc.noaa.gov/geomag/EMM/. cited Jul 31, 2017.

[32] What is a magnetometer? sciencing. https://sciencing.com/about-5397128-magnetometer.html. Accessed Nov. 4, 2021.

[33] Mirko Leomanni. Comparison of control laws for magnetic detumbling. Research Gate, 10 2012. accessed: 2/9/2018.

[34] M. Lovera. Magnetic satellite detumbling: The b-dot algorithm revisited. In 2015 American Control Conference (ACC), pages 1867–1872, July 2015. doi:10.1109/ACC.2015.7171005.

[35] Farhat Assaad. Attitude Determination and Control System for a CubeSat. PhD thesis, Worcester Polytechnic Institute, March 1st 2013.

[36] Amit Sanyal and Zachary Lee-Ho. Attitude tracking control of a small satellite in low earth orbit. Aug 2009. doi:10.2514/6.2009-5902.

[37] Fabio Celani. Robust three-axis attitude stabilization for inertial pointing spacecraft using magnetorquers. ScienceDirect: Acta Astronautica, February–March 2015.

[38] E. Carlen and M.C. Carvalho. Linear Algebra: From the Beginning. W. H. Freeman, 2006.

[39] 1736-1813; Binet Jacques Philippe Marie 1786-1856; Garnier Jean Guillaume 1766-1840 Lagrange, J. L. (Joseph Louis). M´ecanique analytique. Paris, Ve Courcier, 1, 1811.